

Evaluation of Electrode Materials Derived from Walnut Biomass and Their Performance in Sodium-Ion Electrolyte Systems for Sustainable Energy Storage

Tsikritsaki Eleftheria

Department of Electrical and Computer Engineering

Hellenic Mediterranean University

M.Sc. Nanotechnology for Energy Applications

Heraklion, Crete, 2026

Acknowledgments

I would like to express my sincere gratitude to my supervisor, Dr. Dimitra Vernardou, for her continuous guidance, valuable advice, and support throughout the completion of this thesis. Her scientific insight, encouragement, and constructive feedback were essential for the development and completion of this research.

I would also like to sincerely thank PhD candidate Nikos Kavousanos for his invaluable assistance, guidance during the experimental work, and for the many helpful discussions and corrections that greatly contributed to the progress of this study.

I am also grateful to all the collaborators and members of the laboratory for their support, cooperation, and the positive research environment they created during this work.

Finally, I would like to express my deepest gratitude to my family for their unconditional support, patience, and encouragement throughout my academic journey. Their understanding and motivation have been a constant source of strength.

Abstract

The growing demand for sustainable energy-storage technologies has intensified research efforts toward environmentally benign electrode materials and low-cost electrochemical systems. Among emerging solutions, biomass-derived carbons have attracted increasing attention due to their renewability, scalability, and reduced environmental footprint. In this context, the present thesis investigates walnut-shell-derived biochar as a sustainable carbon electrode material for aqueous sodium-based supercapacitor systems, with particular emphasis on the role of electrolyte chemistry in governing electrochemical performance.

Walnut shells were converted into carbon electrodes through a simple activation-free pyrolysis process at 800 °C, followed by pellet fabrication using a PTFE binder. The electrochemical behavior of the produced biochar was systematically evaluated using both three-electrode and symmetric two-electrode configurations in four aqueous sodium electrolytes (Na_2SO_4, $NaNO_3$, NaCl, and NaOH). Cyclic voltammetry and galvanostatic charge–discharge techniques were employed to investigate charge-storage mechanisms, ion transport kinetics, and device-level performance.

The results demonstrate a strong dependence of electrochemical response on electrolyte composition. NaCl and NaOH electrolytes exhibited instability due to corrosion and polarization effects, whereas neutral electrolytes enabled stable capacitive operation. In the three-electrode configuration, $NaNO_3$ delivered higher specific capacitance values (up to 102.4 F g^{-1}) owing to enhanced ion mobility and efficient electric double-layer formation, while Na_2SO_4 promoted more stable and reversible electrochemical behavior. Device-level evaluation in symmetric cells revealed a trade-off between capacitance and durability: although $NaNO_3$ provided higher initial capacitance, Na_2SO_4 exhibited superior long-term stability, retaining approximately 90% of its initial capacitance after 6000 charge–discharge cycles.

Overall, the study demonstrates that electrolyte engineering represents a key strategy for optimizing the performance of activation-free biomass-derived carbon electrodes. The findings highlight the potential of walnut-shell biochar as a low-cost, sustainable material for aqueous sodium-based energy-storage systems and contribute to a deeper understanding of electrolyte–electrode interactions in environmentally responsible supercapacitor technologies.

Keywords: Biomass-derived carbon, walnut-shell biochar, supercapacitors, aqueous sodium electrolytes, electric double-layer capacitors (EDLC), sustainable energy storage, electrochemical characterization, sodium-ion systems, activation-free carbon electrodes

Table of Contents

Acknowledgments....1
Abstract....2
List of Tables....5
List of Figures....6
Chapter 1. Introduction....8
1.1 Growing Demand for Sustainable and Efficient Energy-Storage Systems....8
1.2 Need to Reduce Reliance on Fossil Fuels and Lower Carbon Emissions....9
1.3 Energy Storage Technologies: Emphasis on Sodium-Based Systems and Supercapacitors....11
1.4 Why Sodium-Based Aqueous Electrolytes for Supercapacitors?....13
1.5 Electrode Materials for Supercapacitors Focusing on Carbon Materials....14
1.6 Importance of Low-Cost, Renewable, and Eco-Friendly Electrode Materials for Sustainable Energy-Storage Devices....14
1.7 Current Research Landscape....15
1.8 References....19
CHAPTER 2. Synthesis-Experimental Part....23
2.1 Preparation of Aqueous Sodium Electrolytes....23
2.2 Preparation and Fabrication of Walnut-Shell Biochar Electrodes....24
2.2.1 Biomass collection and pre-treatment....24
2.2.2 Pyrolysis process and post-treatment of activation-free biochars....24
2.2.3 Preparation of Biochar-Based Pellet Electrodes....25
2.3 Experimental Setup....26
2.4 Cyclic Voltammetry – Principles and Applications....27
2.4.1 Cyclic Voltammetry in the Three-Electrode Configuration....28
2.4.2 Cyclic Voltammetry in the Two-Electrode Configuration....29
2.5 Galvanostatic Charge–Discharge (GCD) Method....30
2.6 References....32
Chapter 3. Electrochemical Analysis of Three-Electrode System....33
3.1 Electrochemical Incompatibility of NaCl Electrolyte....33
3.2 Electrochemical Response in NaOH Electrolyte....34
3.3 Galvanostatic Charge–Discharge Behavior in Neutral Electrolytes....35
3.4 Specific Capacitance Analysis....36
3.5 Comparison with Literature....39
3.6 Cyclic Voltammetry Analysis....40

3.7 Scan-Rate Dependence and Ion Transport 42
3.8 Kinetic Analysis Using the Power-Law Relationship 43
3.9 Diffusion- and Surface-Controlled Contributions 45
3.10 EDLC and Pseudocapacitive Contributions 47
3.10.1 Separation of Charge-Storage Components 47
3.10.2 Comparative Analysis of Electrolyte Influence 49
3.11 Discussion about Electrolyte-Dependent Charge Storage Mechanisms: Influence of Ion Chemistry, Conductivity, and pH 50
3.12 References 53
Chapter 4. Two-Electrode System Cell: Electrochemical Analysis 56
4.1 Galvanostatic Charge–Discharge Performance in the Two-Electrode Configuration 56
4.2 Specific Cell Capacitance Comparison in the Two-Electrode System 57
4.3 Comparative Cyclic Voltammetry Analysis 57
4.4 Cycling Stability and Coulombic Efficiency Analysis 58
4.5 Comparison with Literature and Performance Benchmarking 61
4.6 References 63
Chapter 5. Conclusions 64
Chapter 6. Future Perspectives and Research Directions 66

List of Tables

Table 1.1: Comparison of non-activated and activated biochar electrodes tested in neutral aqueous Na_2SO_4 electrolyte. 17
Table 2.1: **:** pH values (experimentally measured at 20 °C) and electrical conductivity ranges (literature values at 20 °C) of the 1 M aqueous sodium-based electrolytes used in this study [1]. 24
Table 3.1: Comparison of biomass-derived carbon electrodes evaluated in aqueous sodium electrolytes using three-electrode configurations..... 39

List of Figures

Figure 1.1 Projected global CO_2 emissions by sector under the IEA Net Zero by 2050 scenario, highlighting the critical role of electrification and renewable energy deployment in achieving deep decarbonization [1]. 8
Figure 1.2 Global CO_2 emissions from fossil fuels and projected trends, illustrating the persistent rise in emissions under business-as-usual scenarios [7]. 10
Figure 1.3 Schematic illustration of charge-storage mechanisms in biomass-derived carbon-based supercapacitors. **(a)** Electric double-layer capacitor (EDLC) mechanism, where charge is stored electrostatically at the electrode–electrolyte interface. **(b)** Comparison between EDLC, pseudocapacitor, and hybrid supercapacitor behaviors, showing characteristic cyclic-voltammetry profiles and ion adsorption processes [15]. 12
Figure 2.1 **a)** Preparation of aqueous sodium-based electrolyte solutions under magnetic stirring, **b)** prepared 1 M NaCl, NaOH, Na_2SO_4 and $NaNO_3$ electrolyte solutions in volumetric flasks. 23
Figure 2.2 Harvesting and pyrolysis procedure for producing biochar based on walnut shell. [3] 25
Figure 2.3 Non-activated biochar. ..... **Σφάλμα! Δεν έχει οριστεί σελιδοδείκτης.**
Figure 2.4 Step-by-step illustration of the walnut-shell biochar pellet fabrication process: **(a)** ground and homogenized walnut-shell-derived biochar powder, **(b)**PTFE binder, **(c)** grinding and mixing of the biochar–binder mixture in an agate mortar, **(d)** formation of a cohesive biochar paste, **(e)** stainless-steel pellet die used for electrode shaping, **(f)** hydraulic press employed for pellet compaction, and **(g)** final free-standing biochar pellets obtained after pressing. 26
Figure 2.5 Swagelok-type two-electrode cell (a) external view and (b) assembled configuration with mounted biochar electrode. 27
Figure 2.6 Representative cyclic voltammogram showing anodic (E_{pa}, i_{pa}) and cathodic (E_pc, i_pc) peaks corresponding to oxidation and reduction processes in a reversible redox system. [5] 28
Figure 2.7 AUTOLAB potentiostat/galvanostat (Metrohm PGSTAT204) used for CV measurements in three-electrode and two-electrode configurations. 28
Figure 2.8 Schematic representation of the three-electrode electrochemical configuration used for cyclic voltammetry measurements. 29
Figure 2.9 Experimental setup showing the assembled two-electrode Swagelok-type cell and its electrical connection to the AUTOLAB PGSTAT204 potentiostat/galvanostat during electrochemical testing. 31
Figure 3.1 Photographic evidence of degradation observed during electrochemical testing in NaCl electrolyte, including corrosion of metallic components and electrolyte discoloration. 34
Figure 3.2 Electrochemical response of walnut biochar electrodes in NaOH electrolyte showing distorted CV behavior caused by polarization effects. 35
Figure 3.3 Galvanostatic charge–discharge curves of walnut biochar electrodes in Na_2SO_4 and $NaNO_3$ electrolytes at different current densities. 36
Figure 3.4 Specific capacitance of walnut biochar electrodes as a function of current density in Na_2SO_4 and $NaNO_3$ electrolytes. 37
Figure 3.5 Cyclic voltammograms of walnut-shell-derived biochar electrodes recorded at scan rates between 5 and 50 mV s^{-1} in Na_2SO_4 and $NaNO_3$ electrolytes. 41
Figure 3.6 Specific capacitance variation as a function of scan rate for Na_2SO_4 and $NaNO_3$ electrolytes. 42

Figure 3.7 Log(i)–log(v) plots used for kinetic analysis ($i = av^b$). The upper graphs correspond to Na_2SO_4, while the lower graphs correspond to $NaNO_3$ electrolyte measurements. 44
Figure 3.8 Quantitative separation of diffusion-controlled and surface-controlled current contributions derived from cyclic voltammetry analysis for **a)** Na_2SO_4 and **b)** $NaNO_3$ electrolytes. 46
Figure 3.9 Determination of capacitance components from scan-rate analysis: **(a),(c)** Na_2SO_4 electrolyte and **(b),(d)** $NaNO_3$ electrolyte. Upper panels show linear fitting used for total capacitance extraction, while lower panels illustrate separation of EDLC and pseudocapacitive contributions. 48
Figure 4.1 Galvanostatic charge–discharge curves of symmetric walnut biochar cells measured at different current densities in **(a)** Na_2SO_4 and **(b)** $NaNO_3$ electrolytes. 56
Figure 4.2 Specific cell capacitance as a function of current density for symmetric walnut biochar cells operating in Na_2SO_4 and $NaNO_3$ electrolytes. 57
Figure 4.3 Cyclic voltammograms of symmetric walnut biochar cells recorded at different scan rates in **(a)** Na_2SO_4 and **(b)** $NaNO_3$ electrolytes 58
Figure 4.4 Cycling stability of symmetric walnut biochar cells in Na_2SO_4 electrolyte showing **(a)** galvanostatic charge–discharge curves and **(b)** cyclic voltammograms recorded at different cycle numbers 59
Figure 4.5 Capacitance retention (%) as a function of charge–discharge cycling number, demonstrating the cycling stability of the electrode material over 6000 cycles, with a final capacitance retention of approximately 85.3%, indicating good long-term electrochemical stability. 60
Figure 4.6 Cycling stability of symmetric walnut biochar cells in $NaNO_3$ electrolyte showing **(a)** evolution of galvanostatic charge–discharge curves and **(b)** cyclic voltammetry response during cycling 61

Chapter 1. Introduction

1.1 Growing Demand for Sustainable and Efficient Energy-Storage Systems

The rapid growth of global energy consumption, driven by industrial development, digitalization, population increase, and the accelerating electrification of transportation, has created an urgent demand for energy-storage technologies that are efficient, reliable, and environmentally sustainable. At the same time, the global energy system is undergoing a fundamental transformation characterized by the increasing penetration of renewable energy sources.

According to projections by the International Energy Agency (IEA), global electricity demand is expected to rise by nearly 50% by 2050, while more than two-thirds of newly installed power-generation capacity will be based on renewable sources [1]. This transition is illustrated in Figure 1.1 [1], which presents the projected evolution of global CO_2 emissions across major sectors under the IEA "Net Zero by 2050" scenario. As shown in Figure 1.1, emissions from electricity and heat production, industry, transport, and buildings are expected to decline significantly, driven primarily by the large-scale deployment of renewable energy technologies, widespread electrification of end-use sectors, and continuous improvements in energy efficiency.

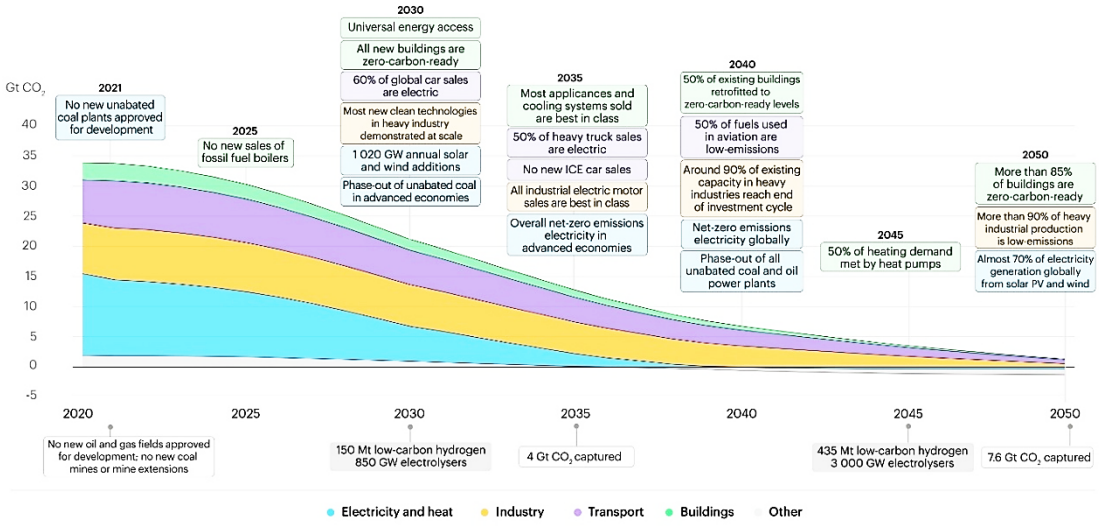


Figure 1.1: Projected global CO_2 emissions by sector under the IEA Net Zero by 2050 scenario, highlighting the critical role of electrification and renewable energy deployment in achieving deep decarbonization [1].

However, Figure 1.1 also highlights a critical challenge associated with this transition: the increasing reliance on variable renewable energy sources. Solar and wind power, despite their environmental advantages, are inherently intermittent and geographically dependent. Solar energy generation is unavailable during nighttime hours, while wind power output fluctuates with meteorological conditions, leading to temporal mismatches between electricity generation and demand [2]. Without effective energy-storage solutions, these fluctuations can compromise grid stability and limit further renewable-energy penetration.

Currently, lithium-ion batteries dominate the markets of portable electronics and electric vehicles due to their high energy density and well-established manufacturing infrastructure. Nevertheless, their strong dependence on critical raw materials such as lithium and cobalt raises significant environmental, economic, and geopolitical concerns, highlighting the urgent need for alternative electrochemical energy-storage technologies based on more abundant and sustainable materials [3].

Among the various energy-storage technologies, supercapacitors, also known as electrochemical capacitors, occupy a distinct position between conventional dielectric capacitors and batteries. Their ability to deliver high power, operate with rapid charge–discharge rates, and sustain long cycle life makes them particularly attractive for applications requiring frequent cycling and fast energy delivery [4].

At the same time, increasing emphasis is being placed on the sustainability of electrode materials employed in energy-storage devices. Carbon-based materials are widely used as supercapacitor electrodes due to their favorable electrical and chemical properties[5], while growing research efforts focus on carbons derived from renewable biomass precursors [6]. Such biomass-derived materials offer a promising pathway toward environmentally responsible solutions by combining low cost, wide availability, and reduced environmental impact.

In this context, biochar derived from walnut shells represents a particularly attractive electrode material for supercapacitor applications, and serves as the main material system explored in the present work to investigate its potential for sustainable and low-cost energy-storage technologies. Walnut shells are an abundant agricultural by-product, and their conversion into functional carbon materials enables the valorization of waste biomass, while supporting the development of sustainable and efficient electrochemical energy-storage technologies. The investigation of supercapacitors employing walnut-biochar-based electrodes therefore aligns with the broader objective of developing sustainable and efficient systems, which is the central focus of the present work.

1.2 Need to Reduce Reliance on Fossil Fuels and Lower Carbon Emissions

For more than a century, fossil fuels have constituted the dominant primary energy sources worldwide, with coal leading global energy supply and accounting for over 80% of electricity generation capacity at the beginning of the 21st century [7]. Although the widespread combustion of fossil fuels has historically supported industrial growth and socioeconomic development, it has also resulted in substantial greenhouse-gas emissions, posing severe and long-term threats to planetary ecosystems.

Atmospheric concentrations of carbon dioxide (CO_2) have now exceeded 420 ppm, reaching levels unprecedented for at least the past three million years [8]. This accumulation has already led to observable environmental consequences, including the accelerated retreat of Himalayan glaciers and the increasing frequency and intensity of extreme climatic events. According to the Intergovernmental Panel on Climate Change

(IPCC), nearly three-quarters of global anthropogenic greenhouse-gas emissions originate directly from fossil-fuel combustion, driving global warming, ocean acidification, and a rising incidence of heat waves, floods, and prolonged droughts.

The persistence of fossil-fuel dependence is further illustrated by long-term emission trends. As shown in Figure 1.2, global annual CO_2 emissions from fossil-fuel combustion have increased steadily since the mid-20th century, reaching historically high levels in recent years. Despite growing awareness of climate change and the gradual deployment of renewable-energy technologies, emissions continue to rise under business-as-usual scenarios, underscoring the structural reliance of modern energy systems on fossil-based fuels [9].

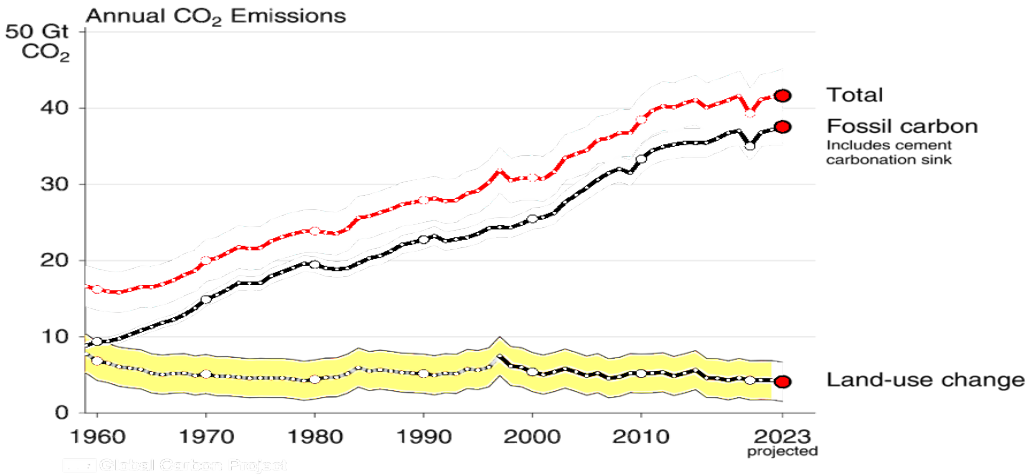


Figure 1.2: Global CO_2 emissions from fossil fuels and projected trends, illustrating the persistent rise in emissions under business-as-usual scenarios [9].

The emission trajectories depicted in Figure 1.2 demonstrate that incremental efficiency improvements alone are insufficient to achieve the reductions required to meet international climate targets, indicating the necessity for a fundamental transformation of the global energy system. In this context, international frameworks such as the Paris Agreement (2015) and the United Nations Sustainable Development Goals (SDG 7 and SDG 13) provide a coordinated roadmap toward low-carbon energy transitions, emphasizing large-scale renewable-energy deployment and enhanced energy efficiency [1].

Nevertheless, the inherently variable and weather-dependent nature of renewable energy sources necessitates complementary technologies capable of decoupling electricity generation from consumption. Energy-storage systems fulfill this role by absorbing excess renewable electricity during periods of surplus production and delivering it when demand exceeds supply, thereby reducing reliance on fossil-fuel-based peaking power plants and enhancing grid flexibility and resilience [10].

Electrochemical energy-storage systems are particularly well suited to addressing these challenges due to their fast response times, high efficiency, and operational flexibility. In parallel, the electrification of end-use sectors—most notably transportation, which

accounts for nearly 25% of global CO_2 emissions—represents a critical pathway toward decarbonization. The replacement of internal combustion engines with electric powertrains supported by advanced batteries or hybrid capacitor technologies offers a direct route toward low-carbon mobility [11], [12].

Achieving truly sustainable electrification requires that energy-storage devices remain environmentally benign throughout their entire life cycle, from raw-material extraction to end-of-life management. Conventional carbon electrode materials often rely on critical or petroleum-based precursors associated with high environmental and economic costs [6], [5]. Consequently, next-generation energy-storage technologies must prioritize both high electrochemical performance and the use of renewable, recyclable, and low-carbon material alternatives.

Biomass-derived carbons are well aligned with these sustainability objectives, as they can be produced from abundant agricultural residues through relatively low-energy processes [13]. Walnut shells, in particular, represent an attractive biomass precursor capable of yielding porous carbon materials with favorable electrochemical characteristics [14]. By utilizing these materials, agricultural waste can be transformed into a valuable resource, providing a sustainable feedstock for next-generation energy-storage devices. When locally available biomass resources are employed, additional environmental benefits arise through reduced transportation requirements and minimized landfill disposal.

1.3 Energy Storage Technologies: Emphasis on Sodium-Based Systems and Supercapacitors

Energy-storage technologies can be broadly classified according to the fundamental mechanisms by which electrical energy is stored and released. Within electrochemical energy-storage systems, two major classes dominate contemporary research and applications: batteries and supercapacitors. Although both rely on electrochemical processes, they differ significantly in their charge-storage mechanisms, performance characteristics, and fields of application [15].

Batteries store energy through faradaic redox reactions that occur within the bulk of the electrode materials. This mechanism enables relatively high energy densities, making batteries suitable for applications requiring sustained energy delivery. However, conventional lithium-ion battery technologies rely on critical raw materials and organic electrolytes, raising concerns related to cost, safety, and long-term sustainability. These limitations have motivated the exploration of alternative charge carriers and device architectures that better align with large-scale, sustainable energy-storage needs.

In this context, sodium has emerged as a particularly attractive alternative to lithium. Owing to its high natural abundance, wide geographical distribution, and low cost, sodium offers clear advantages in terms of resource sustainability and supply-chain security [16]. From an electrochemical standpoint, sodium shares similar intercalation chemistry with lithium, enabling analogous charge-storage mechanisms. Although the larger ionic radius of Na^+ ions (1.02 Å) leads to lower operating voltages and slower diffusion kinetics compared to Li^+, recent advances in electrode nanostructuring and materials engineering have resulted in significant improvements in energy density and

cycling stability [17]. These developments have positioned sodium-based systems as promising candidates for sustainable electrochemical energy storage, particularly when paired with environmentally benign electrolytes.

Beyond batteries, supercapacitors represent a distinct and increasingly important class of electrochemical energy-storage devices. Their surface-controlled charge-storage mechanism enables ultrafast charge–discharge rates, high power density, and exceptional cycling stability. Consequently, supercapacitors are widely used in applications such as regenerative braking in electric and hybrid vehicles, voltage stabilization, power buffering, and hybrid energy-storage systems. In automotive applications, they facilitate efficient recovery of braking energy, reducing fuel consumption, maintenance requirements, and pollutant emissions. In practical systems, supercapacitors operate either as standalone devices for short-term energy storage or as complementary components integrated with batteries [18].

Supercapacitors can be categorized based on their charge-storage mechanisms. Electric double-layer capacitors (EDLCs) store energy via the electrostatic adsorption of ions at the electrode–electrolyte interface, without involving bulk chemical reactions. Pseudocapacitors, by contrast, exploit fast and reversible surface redox reactions that contribute additional capacitance beyond pure electrostatic storage. Hybrid supercapacitors combine features of both EDLCs and pseudocapacitors, typically by integrating a battery-type faradaic electrode with a capacitive non-faradaic electrode, thereby enhancing energy density, while preserving high power performance [5], [19].

The fundamental differences among these mechanisms are schematically illustrated in Figure 1.3, which depicts ion adsorption in EDLCs and contrasts it with pseudocapacitive and hybrid charge-storage behaviors.

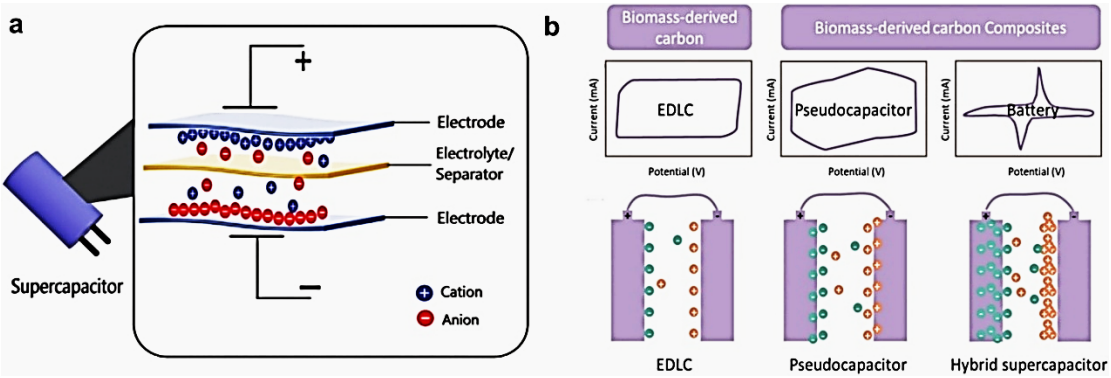


Figure 1.3: Schematic illustration of charge-storage mechanisms in biomass-derived carbon-based supercapacitors. **(a)** EDLC mechanism, where charge is stored electrostatically at the electrode–electrolyte interface. **(b)** Comparison between EDLC, pseudocapacitor, and hybrid supercapacitor behaviors, showing characteristic cyclic-voltammetry profiles and ion adsorption processes [6].

Carbon-based materials dominate supercapacitor technology due to their high electrical conductivity, chemical stability, tunable pore structure, and large specific surface area. In EDLCs, porous carbons provide extensive electrode–electrolyte interfaces that maximize charge storage through ion adsorption. Nevertheless, conventional activated carbons often suffer from limited energy density. To address this limitation, recent

research has focused on biomass-derived porous carbons and heteroatom-doped carbon materials, which combine high surface area with improved wettability and additional redox-active sites [6], [20].

The synergistic control of pore hierarchy and surface chemistry has emerged as a powerful strategy for enhancing the electrochemical performance of carbon electrodes. By integrating micro-, meso-, and macropores with suitable functional groups, biomass-derived carbons can facilitate efficient ion transport, while simultaneously contributing pseudocapacitive effects. This approach bridges the performance gap between batteries and supercapacitors and is particularly promising for sodium-based aqueous energy-storage systems [6].

1.4 Why Sodium-Based Aqueous Electrolytes for Supercapacitors?

In recent years, increasing attention has been directed toward sodium-based aqueous electrolytes as sustainable, non-toxic, and cost-effective alternatives for electrochemical energy-storage devices, particularly supercapacitors [5], [21] . Sodium is the sixth most abundant element in the Earth's crust and is widely available in seawater and natural mineral deposits, ensuring secure supply chains and low material costs [22]. For supercapacitor applications, this abundance translates into scalable and economically viable electrolyte systems, especially when combined with carbon-based electrodes derived from renewable resources. Unlike organic electrolytes commonly used in high-voltage devices, aqueous sodium electrolytes do not involve flammable solvents such as acetonitrile or propylene carbonate, thereby eliminating risks associated with toxicity, leakage, and fire hazards [23].

Neutral aqueous electrolytes, including sodium sulfate (Na_2SO_4), sodium nitrate ($NaNO_3$), and sodium chloride (NaCl), are among the most widely employed electrolyte systems in sodium-based supercapacitors. These electrolytes are inexpensive, easy to prepare, and exhibit high ionic conductivity, typically on the order of 60 mS cm^{-1}, which is approximately one order of magnitude higher than that of conventional organic electrolytes [24]. High ionic conductivity is particularly advantageous for supercapacitors, as it minimizes internal resistance and supports rapid charge–discharge processes.

Although the theoretical electrochemical stability window of water is limited to 1.23 V, appropriate electrode selection and optimized electrolyte conditions can effectively suppress hydrogen and oxygen evolution reactions. As a result, the practical operating voltage window of aqueous supercapacitors can be extended to approximately 1.6 V without compromising device stability. Moreover, the hydrated Na^+ ions exhibit favorable transport kinetics within porous carbon electrode networks, facilitating efficient ion diffusion, reducing charge-transfer resistance, and enhancing rate capability [25].

Aqueous sodium-based electrolytes also provide significant safety advantages. The high heat capacity of water mitigates thermal runaway, while the absence of flammable organic components eliminates fire and explosion risks. These attributes make neutral sodium electrolytes particularly well suited as model systems for evaluating biomass-

derived carbon electrodes within low-cost, environmentally friendly frameworks that align with green-chemistry principles [6]. Furthermore, the simplicity of aqueous electrolyte preparation and handling reduces energy consumption during device fabrication, supporting the development of scalable and sustainable supercapacitor technologies.

1.5 Electrode Materials for Supercapacitors Focusing on Carbon Materials

The electrochemical behavior of a supercapacitor primarily depends on the characteristics of the electrodes; surface area, pore architecture, conductivity, and surface chemistry. Of many candidates such as transition-metal oxides and conducting polymers, carbonaceous materials still rank highest because they provide highest conductivity, structural stability, and low cost [6].

Commercial activated carbons, typically produced from coal, petroleum pitch, exhibit high specific surface areas in the range of 1,000–2,500 $m^2\ g^{-1}$ and demonstrate good rate performance in EDLC configurations [17]. However, their reliance on non-renewable fossil-based precursors and energy-intensive production processes raises concerns regarding long-term sustainability. These limitations have motivated growing interest in renewable carbon alternatives derived from biomass resources.

For carbon electrodes to perform efficiently in supercapacitors, a hierarchical pore structure is essential. Micropores (< 2 nm) provide the primary sites for charge storage by maximizing the accessible surface area, while mesopores (2–50 nm) facilitate rapid ion transport by reducing diffusion resistance within the electrode matrix. The coexistence of these pore regimes enhances capacitance retention at high charge–discharge rates and improves overall power performance [26]. In addition to pore architecture, surface chemistry plays a critical role. Heteroatom doping—through the incorporation of nitrogen, oxygen, sulfur, or phosphorus—improves electrode wettability and modifies the electronic structure of carbon materials, creating additional redox-active sites that contribute pseudocapacitive effects [27].

1.6 Importance of Low-Cost, Renewable, and Eco-Friendly Electrode Materials for Sustainable Energy-Storage Devices

The sustainability of electrochemical energy-storage technologies depends not only on device performance but also on the environmental footprint, cost, and life-cycle impact of the materials employed. While previous sections addressed the growing demand for energy storage and the role of electrochemical systems, the selection of electrode materials emerges as a critical factor governing the feasibility of large-scale and long-term deployment.

Conventional electrode materials are commonly produced through energy-intensive synthesis routes that involve high-temperature treatments, complex chemical processing, and, in many cases, the generation of hazardous by-products [28]. Such processes increase both economic cost and environmental burden, limiting scalability and contradicting the objectives of sustainable energy systems. In addition, many state-

of-the-art electrodes rely on non-renewable or geographically concentrated resources, further constraining supply-chain resilience.

Biomass-derived carbon materials provide a fundamentally different approach by utilizing renewable, low-cost, and widely available feedstocks. Agricultural residues can be converted into functional carbon materials through controlled pyrolysis under oxygen-limited conditions, followed by activation processes designed to tailor porosity and surface characteristics. Depending on the targeted pore structure, activation can be achieved through physical methods (e.g., CO_2 or steam) or chemical treatments (e.g., KOH, $ZnCl_2$, or H_3PO_4) [6]. These processes enable the transformation of low-value biomass into highly porous carbons with large specific surface areas and interconnected pore networks, suitable for electrochemical electrode applications.

Beyond material performance, biomass-derived carbons offer distinct environmental advantages compared to conventional electrodes. The uncontrolled disposal or open-field burning of agricultural residues contributes significantly to greenhouse-gas emissions. Redirecting these waste streams toward biochar production mitigates CO_2 and CH_4 emissions, while simultaneously promoting carbon sequestration, as biochar is a stable carbonaceous material capable of retaining atmospheric carbon over extended timescales [29]. This dual benefit is not typically achievable with synthetic carbons or metal-based electrode materials.

From a life-cycle perspective, biomass-derived carbons further support sustainability through their potential for reuse, regeneration, and recycling. Carbon electrodes generally exhibit high mechanical and electrochemical stability during long-term cycling, in contrast to many transition-metal-based materials that suffer from dissolution, phase transformations, or irreversible degradation. Simple post-treatment strategies, such as thermal annealing or mild chemical washing, can often restore the electrochemical performance of carbon electrodes, reducing waste generation and extending device lifetime [24], [6].

In addition to environmental considerations, biomass-based electrode materials offer important socio-economic benefits. Agricultural residues are inexpensive and geographically widespread, enabling localized production near biomass sources. This reduces transportation-related emissions and costs, while fostering circular-economy models that support rural employment and regional economic development [30]. Such decentralized production pathways are difficult to achieve with conventional electrode materials that depend on centralized, resource-intensive supply chains.

By addressing environmental, economic, and social dimensions simultaneously, these materials form a robust foundation for next-generation energy-storage devices and provide a well-justified materials platform for the systems investigated in the present work.

1.7 Current Research Landscape

In neutral aqueous electrolytes, activated biomass-derived carbons commonly exhibit specific capacitance values in the range of 200–350 F g^{-1} together with excellent cycling stability, typically maintaining more than 90–95% capacitance retention after 10,000 charge–discharge cycles [6], [19], [31], [32].

Among the various biomass precursors investigated for porous carbon production, including coconut shells, rice husks, and bamboo residues, walnut shells have emerged as a particularly promising source due to their dense lignocellulosic structure. This intrinsic structural characteristic facilitates the formation of interconnected micro- and mesoporous carbon networks upon carbonization and activation, which are highly favorable for EDLC applications. Consequently, walnut-shell-derived carbons, including the walnut-shell-derived biochar examined in the present work, typically exhibit high specific surface areas, good mechanical integrity, and favorable surface chemistry, collectively enhancing ion accessibility and charge transport [26], [27].

In the literature, walnut-shell-derived activated carbons have been reported to deliver specific capacitance values exceeding 200–350 F g^{-1} after chemical or physical activation in aqueous electrolytes, while maintaining high coulombic efficiency and stable electrochemical performance over extended cycling, as demonstrated by Pavlenko *et al.* for phosphoric-acid-activated walnut shell carbons exhibiting capacitance values up to 320 F g^{-1} [33], [34].

However, a markedly different performance regime is observed when activation treatments are omitted. The comparative data presented in Table 1.2 reveal that non-activated biochars generally exhibit moderate electrochemical performance in neutral aqueous sodium-based electrolytes. Non-activated biomass carbons derived from sources such as corncob shells and maple display specific capacitance values ranging from approximately 46 to 110 F g^{-1}, depending on pyrolysis temperature and cell configuration [31], [34]. Broader comparative studies further report capacitances of 20–60 F g^{-1} in two-electrode systems and up to 50–130 F g^{-1} in three-electrode configurations for non-activated materials (e.g. corncob shell, maple), whereas activated counterparts (e.g. cellulose-derived carbon, walnut shell, MnO_2@CFB) typically reach 110–350 F g^{-1} under comparable electrolyte conditions [32], [33]. These differences clearly demonstrate the dominant role of activation in increasing electrochemically accessible surface area and enhancing charge-storage efficiency. Activated systems listed in Table 1.2 further reinforce this trend. KOH-activated cellulose-derived carbons exhibit capacitances of 91–117 F g^{-1} [35], while activated walnut-shell carbons achieve approximately 180 F g^{-1} in 1 M Na_2SO_4 using a three-electrode configuration [36]. Modified or composite electrodes, such as MnO_2-decorated carbon fiber biochar, reach intermediate values around 153.9 F g^{-1} [37], indicating that surface functionalization and pseudocapacitive contributions can partially compensate for structural limitations. Additional activated biomass carbons—including pomelo peel, mill sludge, coffee-derived, and wood-derived carbons—exhibit capacitances spanning roughly 46–158 F g^{-1}, depending on testing conditions and current density [38]–[40]. Collectively, these results highlight a broad performance spectrum governed by activation strategy, pore architecture, and electrochemical evaluation methodology.

In contrast, strictly non-activated biomass-derived biochars, similar in nature to the walnut-shell biochar employed in the present study prior to any activation treatment, typically deliver capacitance values below approximately 100 F g^{-1} when tested in 1 M Na_2SO_4 electrolyte. While these values reflect intrinsic limitations associated with lower surface area and reduced pore development, they simultaneously emphasize

important advantages, including simplified processing, reduced energy consumption, low production cost, and environmentally benign synthesis routes. Within this framework, walnut-shell-derived biochar represents a particularly attractive precursor for sustainable supercapacitor electrodes, offering a balance between acceptable electrochemical performance and high material sustainability.

Biomass Precursor	Activation	Pyrolysis (°C)	Electrolyte	Cell Configuration	Specific Capacitance(F/g)	References
Corncob shell	None	700–800	1 M Na_2SO_4	3E	70–110	[36]
Various biomass	None / Activated	–	1 M Na_2SO_4	3E / 2E	50–130 / 20–60 (non-activated) 200–350 (activated)	[37], [38]
Maple	None	900	1 M Na_2SO_4	3E / 2E	46/23	[39]
Cellulose-derived carbon	KOH	_	1 M Na_2SO_4	3E	91-117	[40]
Walnut shell	KOH	-	1 M Na_2SO_4	3E	180	[41]
MnO_2@CFB	Carbon fiber biochar Decorated	-	1 M Na_2SO_4	3E	153.9 (0.5 mA/ g)	[42]
Pomelo peel derived	Biomass-derived activated carbon	-	1 M Na_2SO_4	3E	81.14 (1 A/g)	[43]
Mill Sludge	Activated carbon	-	1 M Na_2SO_4	3E	158 (0.5 A/g)	[44]
Coffee derived Biochar	Activated carbon	-	1 M Na_2SO_4	2E	89 (0.5A/g)	[45]
Wood derived Biochar	Activated carbon	-	1 M Na_2SO_4	2E	46 (5 mA/g)	[45]

Table 1.1: Comparison of non-activated and activated biochar electrodes tested in neutral aqueous Na_2SO_4 electrolyte.

Despite extensive research on biomass-derived carbons, a significant limitation of the current literature lies in the comparatively limited investigation of electrolyte chemistry effects, especially for non-activated biochar systems. Most studies summarized in Table 1.1 evaluate electrodes using a single neutral electrolyte—commonly 1 M Na_2SO_4, which restricts the ability to distinguish whether observed electrochemical behavior originates from intrinsic material properties or electrolyte-dependent phenomena. Electrolyte parameters such as pH, ionic conductivity, anion valence, hydration structure, and ion–surface interactions are expected to strongly influence ion transport

kinetics, polarization behavior, and effective double-layer formation in porous carbon electrodes dominated by EDLC mechanisms.

Within this context, walnut-shell-derived biochar provides an ideal model material for systematically investigating electrolyte effects. Its relatively simple structure, absence of activation-induced complexity, and reproducible synthesis enable isolation of electrolyte-dependent phenomena without significant variations in electrode composition. Therefore, rather than maximizing capacitance exclusively through structural modification, the present work explores electrolyte selection as an alternative pathway for performance optimization.

Accordingly, this study investigates the influence of different aqueous sodium-based electrolytes (Na_2SO_4, $NaNO_3$, NaOH, and NaCl) on the electrochemical behavior of walnut-shell-derived biochar electrodes under identical fabrication and testing conditions. By maintaining constant material properties, while varying electrolyte chemistry, the work seeks to decouple material-driven and electrolyte-driven effects, providing deeper insight into electrolyte–electrode interactions in sustainable aqueous supercapacitor systems. Ultimately, this approach aims to demonstrate that performance improvements in biomass-derived electrodes may arise not only from activation treatments, but also from rational electrolyte engineering.

1.8 References

[1] Dr Fatih Birol , «Net Zero by 2050 A Roadmap for the Global Energy Sector,» International Energy Agency, France, 2021.

[2] I. E. Agency, «Integrating Solar and Wind,» France, 2024.

[3] C. X. e. al., «Future material demand for automotive lithium-based batteries,» *Communications Materials,* 2020.

[4] A. S. e. al., «Supercapacitors for energy storage applications: Materials, devices and future directions: A comprehensive review,» *Journal of Alloys and Compounds,* Vol. 1009, 2024.

[5] P. S. &. Y. Gogotsi, «Materials for electrochemical capacitors,» *Nature Materials,* p. 845–854, 2008.

[6] R. M. Marta Sevilla, «Energy storage applications of activated carbons: supercapacitors and hydrogen storage,» *Energy & Environmental Science,*4, 2014.

[7] C. B. I. e. al., «Trends and Characterization of Primary Energy Sources byEnergy and Food Prices,» *Energies,* 2023.

[8] W. M. Organization, «Greenhouse gas concentrations surge again to new record in 2023,» 2025.

[9] P. F. e. al., «Global Carbon Budget 2023,» *Earth Syst. Sci. Data,* vol. 15, pp. 5301–5369, 2023.

[10] P. D. e. al., «The potential for battery energy storage to provide peaking capacity in the United States,» *Renewable Energy,* Volume 151, pp. 1269-1277, 2020.

[11] B. D. e. al., «Electrical Energy Storage for the Grid: A Battery of Choices,» *Science, vol*. 334, 6058, pp. 928-935, 2011.

[12] I. E. Agency, «Global EV Outlook 2023: Catching up with climate ambitions».

[13] S. B. Wali, «Battery storage systems integrated renewable energy sources: A biblio metric analysis towards future directions,» *Journal of Energy Storage,* 2021.

[14] A. D. e. al., «Carbon nanocomposite electrodes for electrical double layer capacitor,» *Journal of Energy Storage,* Vol. 32, 2020.

[15] Z. L. e. al., «Materials for supercapacitors: When Li-ion battery power is not enough,» *Materials Today,* Vol. 21, Issue 4, pp. 419-436, 2018.

[16] P. P. e. al, «Comprehensive review of Sodium-Ion Batteries: Principles, Materials, Performance, Challenges, and future Perspectives,» *Materials Science and Engineering,* Vol. 312, 2025.

[17] H. Zhang, «Advances in sodium-ion battery cathode materials: exploring chemistry, reaction mechanisms, and prospects for next-generation energy storage systems,» *Journal of Materials Chemistry A,* Issue 45, 2024.

[18] M. E. Şahin, «A Comprehensive Review on Supercapacitor Applications and Developments,» *Energies,* 2022.

[19] L. L. Zhang, «Carbon-based materials as supercapacitor electrodes,» *Chemical Society Reviews,* Vol. 9, 2009.

[20] J. W. e. al., «Recent advances in heteroatoms-doped porous carbon electrode materials for supercapacitors: A review,» *Journal of Energy Storage, vol.* 110, 2025.

[21] T. B. e. al., «To Be or Not To Be Pseudocapacitive?,» *IOP Publishing and The Electrochemical Society,* 2015.

[22] G. W. e. al., «A review of electrode materials for electrochemical supercapacitors,» *Chemical Society Reviews,* Issue 2, 2012.

[23] J.-Y. Hwang, «Sodium-ion batteries: present and future,» *Chemical Society Reviews,* Issue 12, 2017.

[24] P. S. e. al., «Materials for electrochemical capacitors,» *Nature Materials,* p. 845–854, 2008.

[25] L. K. e. al., «Advanced energy materials for flexible batteries in energy storage: A review,» *SmartMat Wiley,* 2020.

[26] M. D. e. al., «Revealing the Impact of Hierarchical Pore Organization in Supercapacitor Electrodes by Coupling Ionic Dynamics at Micro- and Macroscales,» *Advancd Energy Materials,* 2021.

[27] Y. N. e. al., «Sustainable Energy System Planning for an Industrial Zone by Integrating Electric Vehicles as Energy Storage,» *Journal of Energy Storage, vol*. 30, 2020.

[28] G. K. e. al., «Prediction and optimization of machining parameters for minimizing power consumption and surface roughness in machining,» *Journal of Cleaner Production,* vol. 83, pp. 151-164, 2014.

[29] S. M. e. al., «Threats and opportunities for freshwater conservation under future land use change scenarios in the United States,» *Global Change Biology,* Vol. 20, issue 1, 2014.

[30] H. G. e. al., «On the understanding of the mean radiant temperature within both the indoor and outdoor environment, a critical review,» *Renewable and Sustainable Energy Reviews,* volume 117, 2020.

[31] B. K. e. al., «Biochar-based composites as electrode active materials in hybrid supercapacitors with particular focus on surface topography and,» *Journal of Energy Storage,* Volume 39, 2021.

[32] S. C. e. al., «Biochar-based materials for sustainable energy applications: A comprehensive review,» *Journal of Environmental Chemical Engineering.*

[33] A. D. e. al., «Carbon nanocomposite electrodes for electrical double layer capacitor,» *Journal of Energy Storage,* vol. 32, 2020.

[34] V. V. P. e. al., «Temperature Dependent Characteristics of Activated Carbons from Walnut Shells for Improved Supercapacitor Performance,» *Eurasian Chemico-Technological Journal, vol*. 20, 2018.

[35] S. A. e. al, «Walnut Shell Derived N, S Co-Doped Activated Carbon for Solid-State Symmetry Supercapacitor Device,» *Journal of Industrial and Engineering Chemistry, vol*. 129, pp. 309-320.

[36] L. D. e. al., «Corncob-Derived Activated Carbon as Electrode Material for High-Performance Supercapacitor,» *Materials,* 2024.

[37] K. Q. e. al, «Recent advances in utilization of biochar,» *Renew. Sustain. Energy,* pp. 1055-1064, 2015.

[38] Z. Q. e. al., «Biochar-based carbons with hierarchical micro-meso-macro porosity for high rate and long cycle life supercapacitors,» *J. Power Sources,* pp. 82-90, 2018.

[39] L. Y. e. al., "Can Aqueous Na2SO4-Based Neutral Electrolyte Increase Energy Density of Monolithic Wood Biochar Electrode Supercapacitor?," *energies,* 2024.

[40] J. F. e. al., «Symmetric supercapacitors with cellulose-derived carbons and Na2SO4 electrolytes operating in a wide temperature range,» *Journal of Energy Storage,* 2022.

[41] S. A. e. al, «Walnut Shell Derived N, S Co-Doped Activated Carbon for Solid-State Symmetry Supercapacitor Device,» *Journal of Industrial and Engineering Chemistry,* 2023.

[42] S. P. V. H. B. A. G. N. J. S. S. J. M.R. Pallavolu, «High-performance aqueous sodium-ion storage using bundled fiber-based electrodes,» *Journal of Materials Chemistry A,* p. 13354–13367, 2025.

[43] P. L. V. P. N.T. Nguyen, «Biomass-derived activated carbon electrode coupled with a redox additive electrolyte for electrical double-layer capacitors,» *Journal of Nanoparticle Research, vol*. 22, 2020.

[44] K. O. N. G. B. P. T. L. M. M. J. Abdulsalam, «Activated Biocarbon from Paper Mill Sludge as Electrode Material for Supercapacitors: Comparative Performance Evaluation in Two Aqueous Electrolytes,» *ACS Omega, vol*. 8, p. 5285–5299, 2023.

[45] L. A. P. A.-C. F. L.-G. F. M. A. Adan-Mas, «Coffee-derived activated carbon from second biowaste for supercapacitor applications,» *Waste Management, vol*. 120, p. 280–289, 2021.

CHAPTER 2. Synthesis-Experimental Part

2.1 Preparation of Aqueous Sodium Electrolytes

Aqueous sodium-based electrolytes with a concentration of 1 M were prepared using analytical-grade reagents (≥99% purity) and deionized water. Sodium nitrate ($NaNO_3$), ACS, sodium chloride (NaCl), sodium sulfate (Na_2SO_4), Alfa Aesar anhydrous, and sodium hydroxide (NaOH) were selected to investigate the influence of different anions on the electrochemical behavior of the biochar electrodes. For each electrolyte, the required mass of salt was accurately weighed using an analytical balance and dissolved in deionized water in a 100 mL beaker. Magnetic stirring was applied at room temperature until complete dissolution was achieved, as illustrated in Figure 2.1a. Subsequently, the final volume of each solution was adjusted to 100 mL with deionized water, resulting in the prepared 1 M NaCl, NaOH, Na_2SO_4, and $NaNO_3$ electrolyte solutions shown in Figure 2.1b.

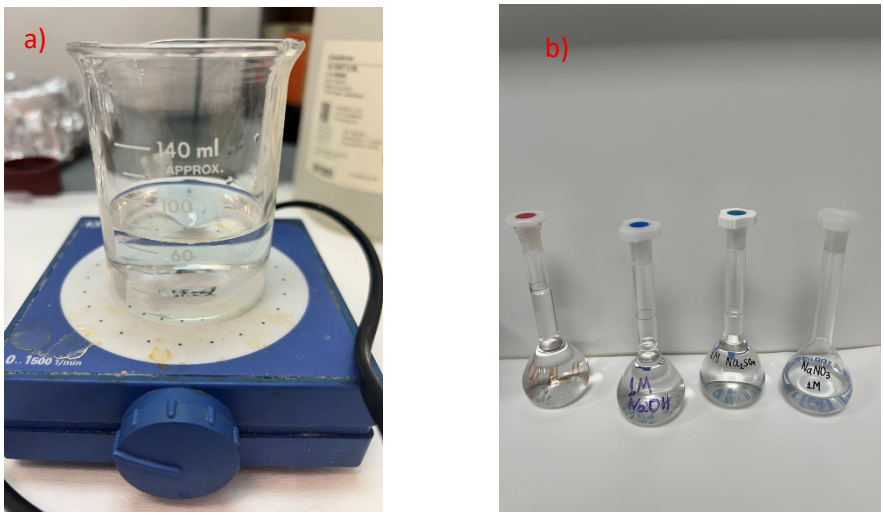


Figure 2.1: **a)** Preparation of aqueous sodium-based electrolyte solutions under magnetic stirring, **b)** 1 M NaCl, NaOH, Na_2SO_4 and $NaNO_3$ aqueous electrolyte solutions in volumetric flasks.

Table 2.1 summarizes the pH values and electrical conductivities of the aqueous sodium-based electrolytes used in this study. The pH values reported, were experimentally measured in the laboratory at 20 °C for each electrolyte solution, providing a direct evaluation of the electrolyte environments employed in the electrochemical experiments. The measured pH values indicate near-neutral conditions for Na_2SO_4 and NaCl, mildly alkaline behavior for $NaNO_3$, and strongly alkaline conditions for NaOH.

The electrical conductivity values reported in Table 2.1 correspond to typical literature ranges for 1 M aqueous sodium-based electrolytes at 20 °C [1]. These values were obtained from standard reference data and peer-reviewed studies in which conductivity is commonly reported as a function of mass percent concentration and subsequently interpolated to the equivalent molar concentration. As shown, NaOH exhibits significantly higher ionic conductivity compared to the neutral sodium salts, which is

attributed to the exceptionally high ionic mobility of hydroxide ions (OH^-) in aqueous media. In contrast, NaCl, $NaNO_3$, and Na_2SO_4 display comparable conductivities within a narrower range, reflecting differences in anion size, charge, and hydration behavior. The reported conductivity ranges provide a reliable benchmark for evaluating ion transport and electrochemical performance in the investigated supercapacitor systems.

Electrolyte	pH	Conductivity
Na_2SO_4	7,03	70–80 mS/cm
$NaNO_3$	8,47	85–95 mS/cm
NaOH	~14	200–250 mS/cm
NaCl	~7	100–110 mS/cm

Table 2.1: **:** pH values (experimentally measured at 20 °C) and electrical conductivity ranges (literature values at 20 °C) of the 1 M aqueous sodium-based electrolytes used in this study [1].

2.2 Preparation and Fabrication of Walnut-Shell Biochar Electrodes

2.2.1 Biomass collection and pre-treatment

The soft inner part of walnut shells was collected from local agricultural producers in Chania, Crete. The raw biomass was air-dried for several days at ambient conditions to remove residual moisture. Subsequently, the dried material was mechanically ground using a conventional knife mill and sieved to obtain particles with a size smaller than 1 mm. This pre-treatment ensured homogeneity of the biomass feedstock prior to the thermal conversion process [2].

2.2.2 Pyrolysis process and post-treatment of activation-free biochars

Pyrolysis was carried out at 800 °C for 60 min under an inert nitrogen atmosphere with a constant flow rate of 0.5 L min^{-1}, using a Carbolite ELF chamber furnace (Figure 2.2). Pre-weighed biomass samples were placed in porcelain crucibles and introduced into the furnace after reaching the target temperature. Following the completion of the pyrolysis process, the furnace was allowed to cool naturally to room temperature under nitrogen flow. The resulting biochar sample was then recovered [2].

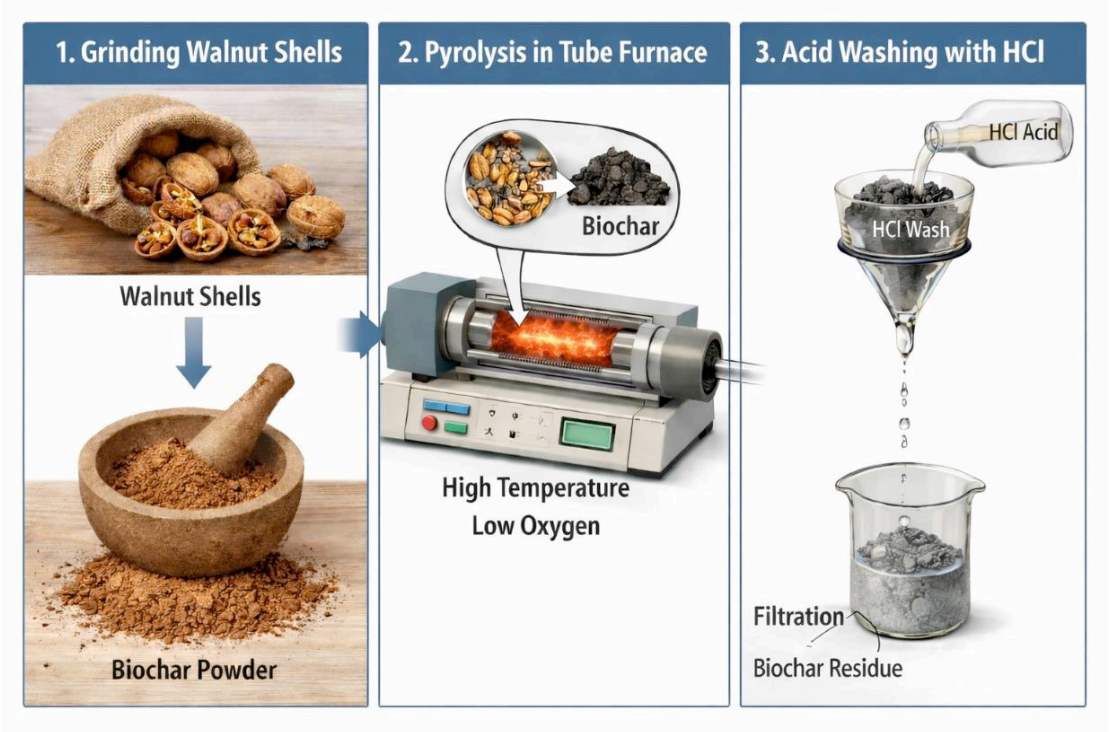


Figure 2.2: Harvesting and pyrolysis procedure for producing biochar based on walnut shell [3].

To reduce the inorganic ash content, walnut biochar sample was washed with 200 mL of 0.1 M HCl, ACS reagent, 37% Sigma Aldrich, followed by repeated rinsing with distilled water until neutral pH (≈7) was achieved. The washed walnut biochar was subsequently dried at 105 °C for 12 h prior to electrode fabrication. [2] No physical or chemical activation step was applied, and the obtained material is therefore referred to as non-activated biochar.

2.2.3 Preparation of Biochar-Based Pellet Electrodes

After completion of the biochar synthesis and post-treatment procedures, the walnut-shell biochar electrodes were prepared through three main stages: (i) pulverization and homogenization of the biochar powder, (ii) incorporation of a binder to form a cohesive paste, and (iii) compaction into peel-like electrode pellets suitable for electrochemical testing.

Initially, for electrode fabrication, 95 mg of the biochar powder (Figure 2.3a) were carefully weighed and transferred to a clean glass dish. The carbon material was then pulverized using an agate mortar and pestle until a homogeneously fine powder was achieved to ensure uniform particle distribution and potentially improve packing density.

To enhance the mechanical stability and preserve the structural integrity of the electrodes during pellet formation, a small amount of polytetrafluoroethylene (PTFE, Teflon) Fluoro Chem, binder was incorporated. Specifically, 5.2 mg of PTFE (Figure 2.3b), corresponding to approximately 5 wt%, were added to the biochar and thoroughly ground together in an agate mortar (Figure 2.3c) to obtain a fine and homogeneous powder as shown in Figure 2.3d. This process enabled uniform dispersion of the binder

throughout the carbon matrix, promoted consistent adhesion between biochar particles, and helped to minimize pore blockage.

The mixture was then placed into a 1 cm diameter die (Figure 2.3e) and compressed under a hydraulic pressure of 500 kg (Figure 2.3f) to form dense electrode pellets. The formed pellets (hereafter referred to as electrodes) exhibited a peel-like morphology with smooth, uniform surfaces (Figure 2.3g).

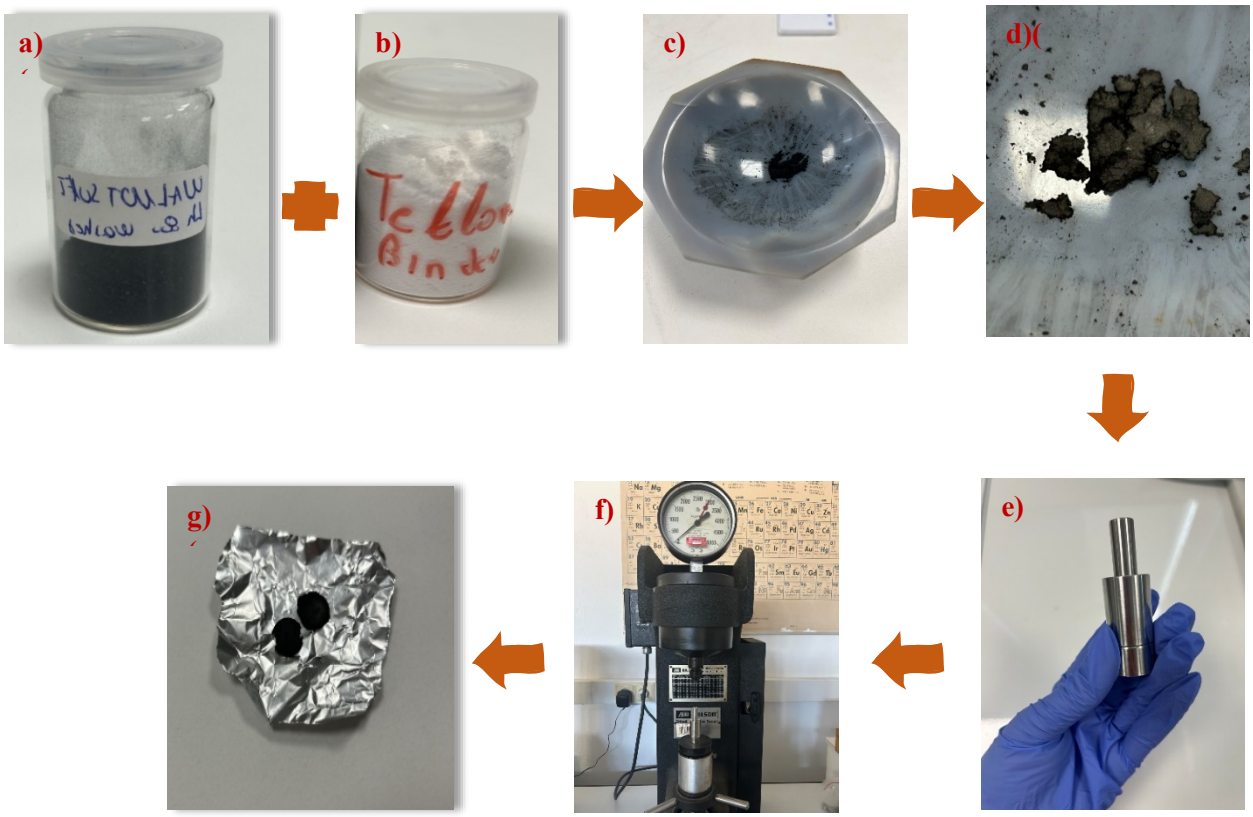


Figure 2.3: Step-by-step illustration of the walnut-shell biochar pellet fabrication process: **(a)** ground and homogenized walnut-shell-derived biochar powder, **(b)** PTFE binder, **(c)** grinding and mixing of the biochar–binder mixture in an agate mortar, **(d)** formation of a cohesive biochar paste, **(e)** stainless-steel pellet die used for electrode shaping, **(f)** hydraulic press employed for pellet compaction, and **(g)** final free-standing biochar pellets obtained after pressing.

The final electrode masses were 25.02 mg and 25.58 mg, corresponding to the two symmetric electrodes used in the electrochemical measurements. The moderate compaction pressure and PTFE ratio resulted in flexible yet mechanically robust electrodes suitable for reproducible assembly and long-term testing.

2.3 Experimental Setup

The fabricated electrodes were assembled into a symmetric two-electrode configuration to evaluate their capacitive performance (Figure 2.4). Two identical walnut-biochar electrodes served as the positive and negative electrodes, separated by a glass-fiber paper (Whatman GF/A) acting as a porous separator. Prior to assembly, the separator was thoroughly soaked in the selected aqueous electrolyte solution (NaCl, NaOH, Na_2SO_4, or $NaNO_3$) to ensure full wetting and effective ionic contact between the

electrodes. The electrolyte-saturated separator was subsequently used for the assembly of the experimental cell under identical conditions for all tested electrolyte compositions [4]. The cell was constructed in a sandwich-like configuration, with the two biochar electrodes positioned on either side of the electrolyte-impregnated separator and gently compressed to ensure full interfacial contact. This setup was used for all electrochemical measurements (Cyclic voltammetry (CV), Galvanostatic Charge–Discharge (GCD)).

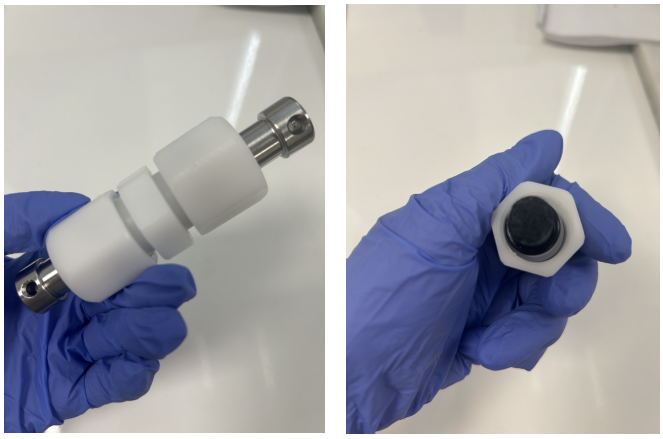


Figure 2.4: Swagelok-type two-electrode cell (a) external view and (b) assembled configuration with mounted biochar electrode.

2.4 Cyclic Voltammetry – Principles and Applications

Cyclic voltammetry (CV) is one of the most fundamental and versatile electrochemical technique used to study the redox properties of materials, reaction mechanisms, and the kinetics of charge transfer processes. It operates by linearly sweeping the potential of an electrode over a defined range and measuring the resulting current response. The plot of current (I) versus potential (E), known as a cyclic voltammogram, provides a direct representation of the electrochemical processes occurring at the electrode–electrolyte interface [5].

During a CV experiment, the applied potential increases from an initial value to a predetermined vertex potential and then reverses, completing a full potential cycle. Depending on the nature of the electrochemical system, the resulting voltammograms may display distinct oxidation and reduction peaks in Faradaic processes or quasi-rectangular shapes characteristic of capacitive behavior [6]. As shown in Figure 2.5, a typical cyclic voltammogram of a reversible redox system presents well-defined anodic and cathodic peaks corresponding to oxidation and reduction processes. The symmetry and shape of the voltammogram provide important information regarding reversibility, reaction kinetics, and capacitive behavior [5].

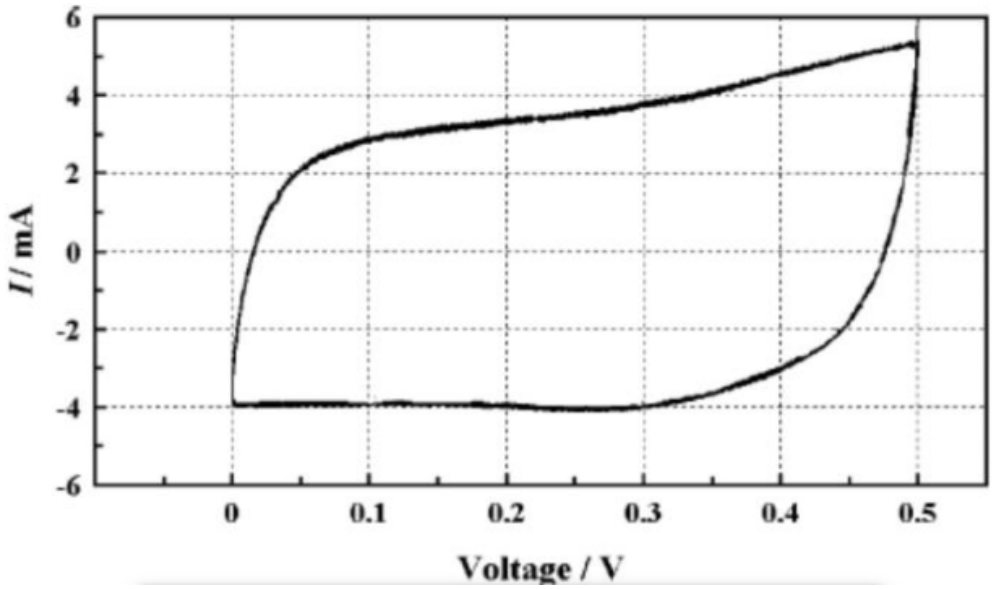


Figure 2.5: Representative cyclic voltammogram showing anodic (E_{pa}, i_{pa}) and cathodic (E_pC, i_pC) peaks corresponding to oxidation and reduction processes in a reversible redox system [5].

All cyclic voltammetry measurements in this study were conducted using an AUTOLAB PGSTAT204 potentiostat/galvanostat (Metrohm), (Figure 2.6), controlled by NOVA software, ensuring precise potential control and current acquisition.

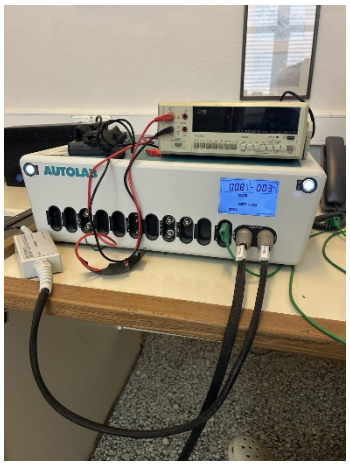


Figure 2.6: AUTOLAB potentiostat/galvanostat (Metrohm PGSTAT204) used for CV measurements in three-electrode and two-electrode configurations.

2.4.1 Cyclic Voltammetry in the Three-Electrode Configuration

CV measurements were carried out using a three-electrode electrochemical system to characterize the capacitive behavior of the walnut-shell biochar electrodes. This configuration allows precise control of potential and current, ensuring accurate assessment of the electrochemical response of the working electrode.

The experimental setup consisted of a biochar pellet as the working electrode, a silver/silver chloride (Ag/AgCl, 3 M KCl) reference electrode, and a platinum foil serving as the counter electrode as shown in Figure 2.7. Typical electrolytes used in this study included $NaNO_3$, Na_2SO_4, NaCl, and NaOH. These electrolytes provide an

excellent ionic transport and compatibility with carbon-based electrodes, making them ideal candidates for sustainable electrochemical systems [4]. Prior to measurements, the electrolyte solutions were deaerated to remove dissolved oxygen and equilibrated under ambient temperature and pressure to minimize parasitic reactions.

Cyclic voltammetry measurements were performed by linearly sweeping the applied potential between −0.8 and +0.8 V vs. Ag/AgCl at scan rates ranging from 5 to 50 mV s^{-1}, selected according to the specific experimental requirements, while recording the corresponding current response. The obtained current–potential plots (cyclic voltammograms) provide insight into the electrochemical response of the electrode–electrolyte system and the capacitive behavior associated with charge storage at the electrode–electrolyte interface.

The specific capacitance (C_s) was calculated from the cyclic voltammetry data using Equation (1) [7]:

$$C_s = \frac{1}{2m\Delta V v} \int I(V)\, dV \quad \textbf{(1)}$$

where m (g) is the mass of the active electrode material, ΔV (V) is the potential window, v (V s^{-1}) is the scan rate, and $I(V)$ (A) is the measured current as a function of potential. The factor of ½ accounts for the two charge–discharge sweeps during one complete potential cycle.

The measurements were repeated to ensure reproducibility, and each voltammogram was corrected for background current prior to analysis. All experiments were performed at room temperature (≈ 25 °C) under ambient laboratory conditions.

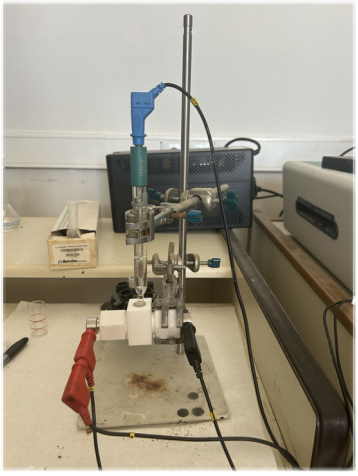


Figure 2.7: Schematic representation of the three-electrode electrochemical configuration used for cyclic voltammetry measurements.

2.4.2 Cyclic Voltammetry in the Two-Electrode Configuration

Cyclic voltammetry measurements were also performed using a two-electrode configuration, which more closely represents the actual operating conditions of a full

supercapacitor cell. For measurements performed in a two-electrode configuration, the experimental setup was identical to that described above, with the exception that no reference electrode was employed. Two identical walnut-shell-derived biochar pellets were used as the positive and negative electrodes and were separated by a glass fiber paper separator soaked in the corresponding aqueous sodium electrolyte ($NaNO_3$, Na_2SO_4, NaCl, or NaOH). The assembly was housed in a Swagelok-type Teflon cell, with stainless steel end fittings serving as current collectors and providing uniform mechanical pressure on the electrode stack.

The voltage was cycled symmetrically within a total voltage window of 0–1 V, while the resulting current response was recorded to obtain the corresponding cyclic voltammograms. This voltage range was selected to avoid water decomposition and ensure stable operation of the aqueous electrolyte systems [4], [7].

The cell capacitance (C) of the full device was calculated from the corresponding galvanostatic charge–discharge (GCD) profiles using Equation (2) [7]:

$$C = \frac{I\,\Delta t}{m\,\Delta V} \quad \textbf{(2)}$$

where I (A) is the applied current, Δt (s) is the discharge time, m (g) is the combined mass of both electrodes, and ΔV (V) is the applied voltage window. This expression provides a reliable measure of the total capacitance of the symmetric device, accounting for both electrodes simultaneously.

All electrochemical measurements were carried out at room temperature (≈ 25 °C) under ambient conditions. After completion of the full set of measurements for each electrolyte system, the cell was disassembled, thoroughly rinsed with deionized water, and dried before being reassembled for the subsequent electrolyte. This procedure was applied systematically to ensure reproducibility and to prevent cross-contamination between different electrolyte compositions.

2.5 Galvanostatic Charge–Discharge (GCD) Method

The galvanostatic charge–discharge technique is a fundamental electrochemical method widely used to evaluate the capacitive performance, reversibility, and efficiency of energy-storage devices such as supercapacitors. In this technique, a constant current is applied to the cell, and the resulting voltage variation with time is recorded during successive charge and discharge cycles [8]. Unlike cyclic voltammetry, which provides qualitative information about charge-storage mechanisms, GCD offers a direct quantitative measurement of capacitance, energy density, and coulombic efficiency.

During the charging process, ions from the electrolyte accumulate on the surface of the electrode (or participate in fast surface redox reactions in pseudocapacitive systems). When the current direction is reversed, these ions are released, producing the discharge curve. The linear and nearly symmetrical charge–discharge profiles typically indicate ideal EDLC behavior, whereas deviations from linearity may imply pseudocapacitive contributions or resistive losses.

All GCD measurements in this study were performed using the same system as before controlled by NOVA software. The assembled two-electrode Swagelok-type cell was connected as shown in Figure 2.8, with the positive and negative terminals attached to the respective stainless-steel current collectors. The experiments were conducted under ambient laboratory conditions (≈ 25 °C) using the same sodium-based aqueous electrolytes as before.

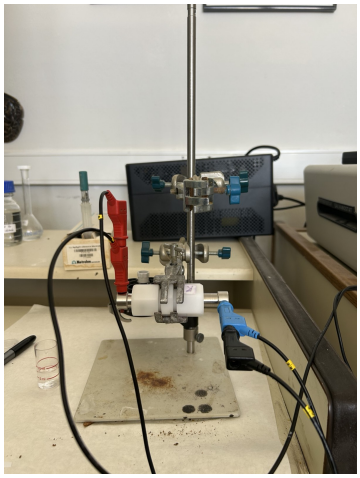


Figure 2.8: Experimental setup showing the assembled two-electrode Swagelok-type cell and its electrical connection to the AUTOLAB PGSTAT204 potentiostat/galvanostat during electrochemical testing.

Each device was charged and discharged within a fixed voltage window of 0–1 V at different specific currents ranging from 0.1 A g^{-1} to 0.5 A g^{-1}, depending on the test sequence. The potential and current data were continuously recorded to generate the corresponding GCD curves (voltage vs. time).

2.6 References

[1] R. C. Weast, CRC Handbook of Chemistry, and Physics, 70th Edition, CRC Press, Boca Raton, FL, 1989, p. D-221..

[2] M. A. e. al., Sustainable Choices for Energy Storage: Assessing Electrode-Relevant Properties of Biomass-Derived Materials, 2025.

[3] E. T. D. K. D. V. Nikos Kavousanos, «Walnut Soft derived biochar as a sustainable carbon,» 2026.

[4] Y. G. Patrice Simon, «Materials for Electrochemical Capacitors,» *PubMed,* 2018.

[5] A. J. &. F. L. R. Bard, Electrochemical methods: fundamentals and applications. New York: Wiley., New York: Wiley., 2001.

[6] J. Wang, Analytical electrochemistry, New York: Wiley-VCH., 2006.

[7] B. E. Conway, Electrochemical Supercapacitors: Scientific Fundamentals and Technological Applications., New York, 1999.

[8] M. D. S. a. R. S. Ruoff, «Best practice methods for determining an electrode material's performance for ultracapacitors,» *Energy and Environmental Science, vol.* 9, 2010.

Chapter 3. Electrochemical Analysis of Three-Electrode System

This chapter presents the electrochemical investigation of walnut-shell-derived biochar electrodes using a three-electrode configuration in order to evaluate their intrinsic electrochemical behavior. Building upon the experimental methodology described in Chapter 2, the study examines the effect of aqueous sodium-based electrolytes (NaCl, NaOH, Na_2SO_4, and $NaNO_3$) on ion transport processes and electrode–electrolyte interactions under identical experimental conditions. Cyclic voltammetry and galvanostatic charge–discharge measurements are employed to analyze the kinetic characteristics and charge-storage mechanisms governing the observed response.

The comparative analysis revealed that electrolyte selection strongly influences the electrochemical operation of the system, as not all electrolytes exhibited compatible behavior with the biochar electrodes. Marked differences were observed in reversibility and overall response, emphasizing the decisive role of electrolyte composition in aqueous carbon-based electrochemical systems. The chapter therefore begins with evaluation of electrolyte compatibility, followed by detailed comparison of neutral electrolyte systems and analysis of scan-rate effects, kinetic parameters, and the relative contributions of electric double-layer and pseudocapacitive processes, providing a comprehensive framework for understanding charge storage in biomass-derived carbon electrodes.

3.1 Electrochemical Incompatibility of NaCl Electrolyte

Electrochemical testing in NaCl electrolyte resulted in rapid degradation of the experimental system. Shortly after polarization began, corrosion phenomena became evident on metallic components of the electrochemical cell, accompanied by progressive discoloration of the electrolyte solution. As shown in Figure 3.1, the electrolyte gradually developed a brown coloration while visible deterioration appeared on the current collectors and electrode assembly.

This behavior is attributed to chloride-induced corrosion processes. Chloride ions are well known to penetrate and destabilize passive oxide layers formed on metallic surfaces, promoting localized anodic dissolution through the formation of soluble metal–chloride complexes [1]. Under electrochemical polarization, these reactions are significantly accelerated, leading to the formation of hydroxides and oxides that cause electrolyte discoloration and increased interfacial resistance. Similar degradation mechanisms in chloride-containing electrolytes have been widely reported in electrochemical systems and corrosion studies [2].

The accumulation of corrosion products disrupts electrical contact between the electrode and current collector, resulting in unstable current response and preventing reliable cyclic voltammetry measurements. Such behavior highlights that electrolyte compatibility in aqueous electrochemical systems depends not only on ionic conductivity but also on chemical stability and corrosion interactions between the electrolyte and cell components [3].

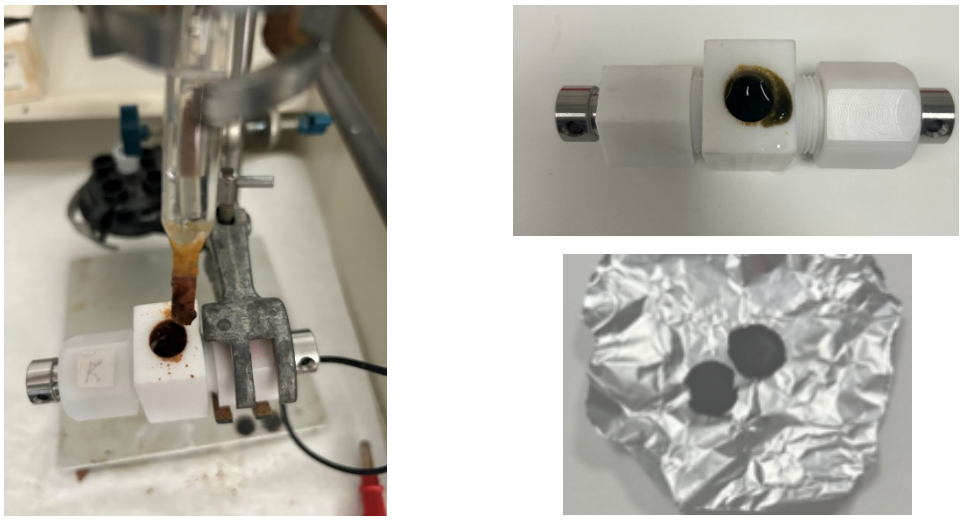


Figure 3.1: Photographic evidence of degradation observed during electrochemical testing in NaCl electrolyte, including corrosion of metallic components and electrolyte discoloration.

The observed behavior demonstrates that electrolyte compatibility depends not only on ionic conductivity but also on chemical interactions with cell components.

3.2 Electrochemical Response in NaOH Electrolyte

Measurements performed in NaOH electrolyte exhibited strongly non-ideal electrochemical behavior. The system could not sustain specific currents higher than 0.1 A g^{-1} without pronounced polarization effects. The electrochemical response, illustrated in Figure 3.2, shows distorted cyclic voltammograms and non-linear galvanostatic charge–discharge profiles. In particular, increased internal resistance and the presence of competing electrochemical processes are observed. Several physicochemical factors may account for this behavior. First, strongly alkaline electrolytes reduce the effective electrochemical stability window of aqueous systems due to the onset of hydrogen and oxygen evolution reactions at relatively low overpotentials. Gas evolution at the electrode–electrolyte interface may partially block active sites and impede ion transport, resulting in increased polarization and non-ideal capacitive response, as reported by Zhang et al. in studies of aqueous supercapacitors employing porous carbon materials [4]. Second, hydroxide ions interact strongly with oxygen-containing functional groups naturally present on biomass-derived carbons. Surface functionalities such as hydroxyl, carbonyl, and carboxyl groups may undergo deprotonation in alkaline media, altering surface charge density and modifying adsorption energetics. Such chemical interactions can suppress reversible ion adsorption and introduce resistive contributions to the electrochemical response, as discussed by Frackowiak and Béguin for carbon electrodes in alkaline electrolytes [5]. Additionally, although NaOH exhibits high bulk ionic conductivity, the effective ion transport within porous carbon structures depends on ion solvation and accessibility to micropores rather than conductivity alone. Strong hydration of hydroxide ions increases their effective hydrated radius, limiting penetration into narrow pores and reducing utilization of internal surface area. Similar transport limitations in alkaline electrolytes have been reported by Simon and Gogotsi in their analysis of porous carbon supercapacitors [6]. Furthermore, alkaline environments may promote side reactions involving surface oxidation or reconstruction of carbon functional groups, contributing to irreversible current components and distorted voltametric profiles [7].

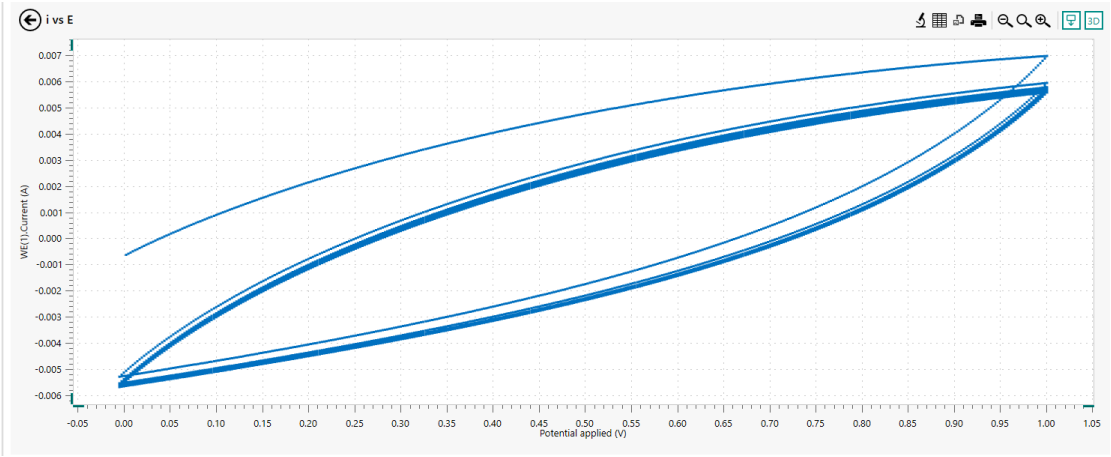


Figure 3.2: Electrochemical response of walnut biochar electrodes in NaOH electrolyte showing distorted CV behavior caused by polarization effects.

Despite its high ionic conductivity, the combined effects of gas evolution, surface chemistry modification, and restricted ion accessibility within the porous electrode structure limit efficient capacitive operation in NaOH electrolyte.

3.3 Galvanostatic Charge–Discharge Behavior in Neutral Electrolytes

Stable electrochemical performance was achieved when neutral electrolytes (Na_2SO_4 and $NaNO_3$) were employed. Representative galvanostatic charge–discharge (GCD) curves are presented in Figure 3.3. As shown in the figure, both electrolytes exhibit symmetric and nearly linear charge–discharge profiles, indicating highly reversible capacitive behavior dominated by electrostatic ion adsorption at the electrode–electrolyte interface, as commonly reported for porous carbon electrodes operating through electric double-layer capacitance mechanisms [4], [6].

The nearly triangular shape of the GCD curves originates from the constant-current charging process, where charge accumulation occurs via reversible formation of the electrical double layer rather than faradaic phase transformations. In ideal capacitive systems, the voltage varies linearly with time because the stored charge is directly proportional to the applied current, a behavior widely observed in carbon-based supercapacitors [5].

At lower specific currents, longer discharge times were recorded, reflecting efficient ion diffusion throughout the porous electrode structure. Under slow polarization conditions, electrolyte ions have sufficient time to penetrate micropores and mesopores, enabling full utilization of the internal surface area available for charge storage. Similar diffusion-controlled behavior has been reported by Simon and Gogotsi, [6], who demonstrated that ion accessibility within porous carbons strongly depends on the relationship between diffusion time and charging rate.

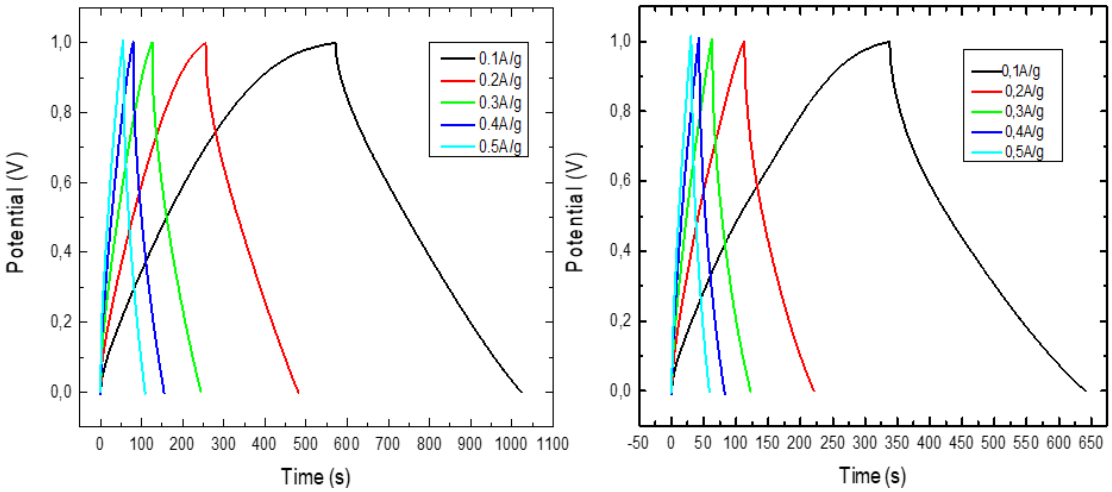


Figure 3.3: Galvanostatic charge–discharge curves of walnut biochar electrodes in Na_2SO_4 and $NaNO_3$ electrolytes at different specific currents.

As the applied specific current increases, discharge duration decreases due to kinetic limitations associated with ion transport inside narrow pores. At higher currents, the characteristic charging time becomes shorter than the diffusion time required for solvated ions to access deeper pore regions. Consequently, charge storage becomes increasingly restricted to external surfaces and larger pores, reducing the effective capacitance. This rate-dependent behavior is characteristic of porous electrode systems and has also been extensively described by Dunn et al. in studies of electrochemical energy storage mechanisms [7].

The preservation of curve symmetry further indicates low internal resistance and minimal polarization losses within the investigated potential window for both electrolytes. However, a comparison between the two systems reveals noticeable differences in electrochemical performance. The $NaNO_3$ electrolyte exhibits longer discharge times at identical specific currents, indicating a higher stored charge and therefore greater specific capacitance compared to the Na_2SO_4 system. This behavior suggests improved ion accessibility and more efficient charge storage processes in the nitrate-based electrolyte. In contrast, the Na_2SO_4 electrolyte displays shorter discharge durations, reflecting lower capacitance under identical operating conditions. Such differences can be attributed to the distinct physicochemical properties of the electrolyte ions, including ionic mobility, hydrated ion size, and interaction with surface functional groups of the biochar electrode. Neutral aqueous electrolytes generally promote stable ion adsorption–desorption processes and suppress parasitic reactions, enabling efficient electrical double-layer formation, as discussed by P. Simon and Y. Gogotsi [6].

3.4 Specific Capacitance Analysis

The dependence of specific capacitance on the specific current for the investigated neutral electrolytes is presented in Figure 3.4. The results were calculated from galvanostatic charge–discharge measurements using Equation (2) in Chapter 2, allowing direct comparison of the charge-storage capability of walnut-shell-derived biochar electrodes in Na_2SO_4 and $NaNO_3$ electrolytes.

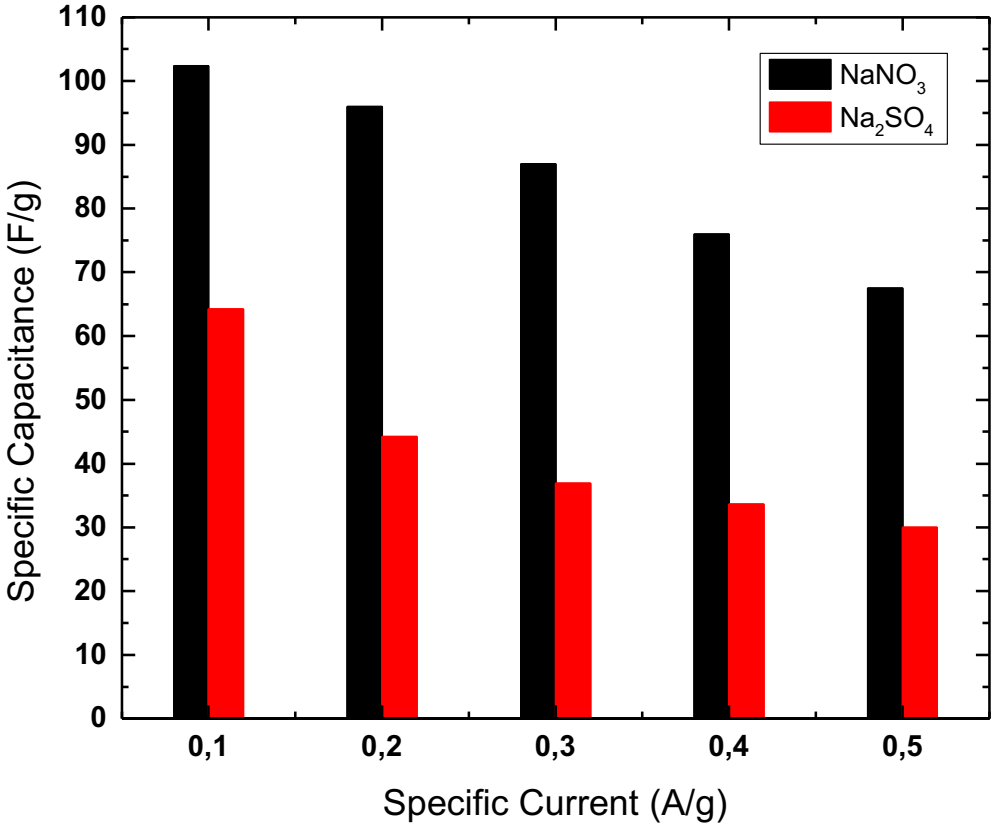


Figure 3.4: Specific capacitance of walnut biochar electrodes as a function of specific current in Na_2SO_4 and $NaNO_3$ electrolytes.

As shown in Figure 3.4, the specific capacitance decreases progressively with increasing specific current for both electrolytes. This behavior is characteristic of porous carbon electrodes and is commonly attributed to ion diffusion limitations within microporous structures [4], [6]. At low specific currents, electrolyte ions have sufficient time to penetrate deeply into the internal pore network, enabling utilization of a larger electrochemically active surface area. In contrast, at higher currents, the timescale of ion transport becomes insufficient for full pore accessibility, restricting charge storage primarily to outer surface regions.

A significant difference between the two electrolytes is observed across the entire specific current range. The $NaNO_3$ electrolyte delivers consistently higher capacitance values, reaching approximately 102.4 F g^{-1} at 0.1 A g^{-1}, compared to 64.2 F g^{-1} for Na_2SO_4. Even at elevated specific currents, $NaNO_3$ maintains superior performance, indicating more efficient ion transport and charge propagation throughout the porous electrode. The enhanced capacitance observed in $NaNO_3$ originates primarily from electrolyte-dependent transport properties. In aqueous systems, nitrate (NO_3^-) is a monovalent anion, whereas sulfate (SO_4^{2-}) is divalent and exhibits higher charge density. Differences in ionic charge and hydration structure strongly influence effective mobility and diffusion in confined porous environments [8]. Monovalent nitrate ions typically possess weaker ion–solvent interactions, forming less rigid hydration shells that facilitate partial desolvation near the electrode surface. This process reduces transport resistance and enables ions to access smaller micropores, thereby increasing the fraction of active surface participating in electric double-layer formation. In

contrast, sulfate ions are strongly hydrated due to their higher electrostatic charge, resulting in a larger effective hydrated radius. These stronger ion–water interactions hinder their diffusion through narrow pores and reduce ion accessibility under dynamic charging conditions. Consequently, only a part of the internal surface contributes effectively to charge storage at increasing current densities, leading to lower measured capacitance values.

The experimental discharge-time data further support this interpretation. As shown previously in Figure 3.3, $NaNO_3$ exhibits systematically longer discharge durations compared to Na_2SO_4 at identical applied currents. Since capacitance is directly proportional to discharge time under constant current conditions, the longer Δt values directly translate into higher calculated capacitance.

Beyond transport kinetics, electrolyte composition may also influence interfacial charge storage through ion–surface interactions. Electrolyte ions can interact differently with the oxygen-containing functional groups commonly present on the surface of biomass-derived carbons such as biochar. According to previous studies, the physicochemical properties of the electrolyte—including ion size, hydration shell, and specific adsorption behavior—can significantly affect the formation of the electrical double layer and the overall capacitance of carbon electrodes [8], [9]. In particular, nitrate ions have been reported to exhibit favorable interactions with carbon surfaces and oxygen-containing functional groups, which may enhance wettability and facilitate ion adsorption at the electrode interface [10], [11]. In contrast, multivalent anions such as sulfate may experience stronger solvation and steric constraints that can limit their accessibility within porous carbon structures. Although these mechanisms cannot be directly confirmed from the present measurements, the slightly improved electrochemical response observed in nitrate-based electrolytes may be consistent with trends reported in the literature.

From a mechanistic perspective, the results indicate that capacitive performance is governed by a balance between ion mobility and ion–surface interaction strength. Faster ionic transport in $NaNO_3$ enables rapid establishment of the electrical double layer across a larger surface fraction, increasing measured capacitance. Meanwhile, the stronger hydration and slower diffusion of SO_4^{2-} ions limit charge storage efficiency despite stable electrochemical behavior [12]. Therefore, the higher capacitance obtained in $NaNO_3$ can be interpreted as the combined outcome of:

1. enhanced ionic mobility and reduced transport resistance,
2. improved accessibility of microporous regions, and
3. electrolyte-dependent interfacial interactions controlling effective surface utilization.

These findings confirm that electrolyte chemistry plays a determining role in maximizing the electrochemical performance of biomass-derived carbon electrodes, even when electrode composition and testing conditions remain identical.

3.5 Comparison with Literature

To place the electrochemical performance of the walnut-shell-derived biochar electrodes investigated in this work into a broader scientific context, a comparative analysis with previously reported biomass-derived carbon materials was conducted. Particular attention was given to studies employing aqueous Na_2SO_4 electrolytes and three-electrode configurations, as these experimental conditions are widely used to evaluate the intrinsic electrochemical properties of carbon-based electrode materials.

Table 3.1 summarizes representative studies reported in the literature for biomass-derived carbon electrodes tested in neutral aqueous electrolytes. The comparison includes key parameters such as biomass precursor type, activation treatment, electrolyte composition, electrochemical configuration, specific capacitance, and cycling stability. Focusing on three-electrode measurements provides a consistent framework for evaluating the fundamental charge-storage capability of the materials, independent of device-level constraints typically encountered in two-electrode systems.

Biomass Precursor	**Activation**	**Pyrolysis (° C)**	**Electrolyte**	**Cell Configuration**	**Specific Capacitance(F/g)**	**Cycling Stability**	**References**
Corncob shell	KOH	–	1 M Na_2SO_4	3E	70–110	90%	[13]
Various biomass	None / Activated	–	1 M Na_2SO_4	3E	50–110 **(non-activated)** 200–350 **(activated)**	–	[14], [15]
Maple	None	900	1 M Na_2SO_4	3E	46	_	[16]
Cellulose-derived carbon	KOH	–	1 M Na_2SO_4	3E	91-117	95 %(2000 cycles)	[17]
Walnut shell	KOH	-	1 M Na_2SO_4	3E	180	95% (5000 cycles)	[18]
MnO_2@CFB	Carbon fiber biochar Decorated	-	1 M Na_2SO_4	3E	153.9 (0.5 mA/ g)	10000	[19]
Pomelo peel derived	Biomass-derived activated carbon	-	1 M Na_2SO_4	3E	81.14 (1 A/g)	5000	[20]
Mill Sludge	Activated carbon	-	1 M Na_2SO_4	3E	158 (0.5 A/g)	5000	[21]
Walnut shell	None	800	1 M Na_2SO_4	3E	34	6000	This work
Walnut shell	None	800	1 M $NaNO_3$	3E	102,4	500	This work

Table 3.1: Comparison of biomass-derived carbon electrodes evaluated in aqueous sodium electrolytes using three-electrode configurations.

As shown in Table 3.1, biomass-derived carbon materials generally exhibit specific capacitance values ranging between approximately 70 and 160 F g^{-1} in neutral Na_2SO_4 electrolytes when chemical activation is applied. Chemical activation treatments, particularly KOH activation, are widely used to enhance the electrochemical performance of biomass carbons by significantly increasing surface area and micropore volume. For example, activated walnut-shell-derived carbon electrodes have been reported to reach capacitance values of approximately 180 F g^{-1} [18], while other activated biomass carbons such as mill-sludge-derived carbon and MnO_2-decorated carbon fiber biochar demonstrate capacitance values exceeding 150 F g^{-1} under comparable experimental conditions [19], [21].

In contrast, the walnut-shell-derived biochar investigated in the present study was synthesized without chemical activation, resulting in a more moderate specific surface area and a less developed microporous structure. Consequently, the measured capacitance of 34 F g^{-1} in Na_2SO_4 electrolyte is comparable to values reported in literature for non-activated biomass-derived carbons investigated under similar aqueous conditions. Although untreated biochars typically exhibit lower capacitance than chemically activated carbons due to their reduced surface area and pore development, the value obtained in this work remains within the range expected for activation-free biomass carbons. These results therefore confirm that even without chemical activation, walnut-shell-derived biochar can provide effective electrochemical charge storage when appropriately integrated into aqueous supercapacitor systems.

Interestingly, when the electrolyte is replaced with $NaNO_3$, the capacitance increases significantly to 102.4 F g^{-1}, highlighting the strong influence of electrolyte chemistry on charge-storage performance. Although most literature studies focus on Na_2SO_4 electrolytes, the present results demonstrate that electrolyte selection can substantially modify ion transport behavior and interfacial charge storage, even when the electrode material and structural properties remain unchanged.

Overall, the comparative analysis indicates that the electrochemical performance of the walnut-shell biochar developed in this work is consistent with the expected behavior of non-activated biomass-derived carbon electrodes. At the same time, the substantial capacitance improvement observed in $NaNO_3$ electrolyte suggests that optimizing electrolyte composition represents an effective strategy for enhancing the performance of sustainable carbon materials without requiring additional chemical activation steps.

These findings provide a useful reference framework for the interpretation of the two-electrode device performance discussed in the following chapter.

3.6 Cyclic Voltammetry Analysis

Cyclic voltammetry measurements were performed at scan rates ranging from 5 to 50 mV s^{-1} in order to evaluate the charge-storage mechanism and kinetic response of walnut-shell-derived biochar electrodes in neutral aqueous electrolytes. The corresponding cyclic voltammograms are presented in Figure 3.5.

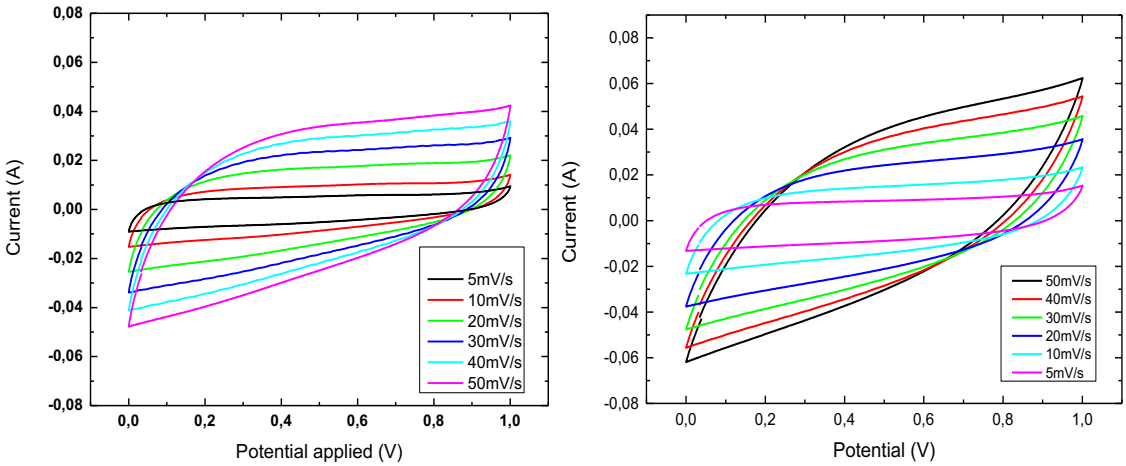


Figure 3.5: Cyclic voltammograms of walnut-shell-derived biochar electrodes recorded at scan rates between 5 and 50 mV s^{-1} in Na_2SO_4 and $NaNO_3$ electrolytes.

As shown in Figure 3.5, both Na_2SO_4 and $NaNO_3$ electrolytes exhibit quasi-rectangular voltammetric profiles, which are characteristic of EDLC behavior typically observed in porous carbon electrodes [5], [6]. The nearly symmetric current response between forward and reverse scans indicates highly reversible ion adsorption and desorption processes at the electrode–electrolyte interface. Such behavior confirms that charge storage is primarily governed by electrostatic accumulation of ions rather than faradaic battery-type reactions, consistent with the expected response of biomass-derived carbon materials possessing developed surface area and accessible porosity [4].

As observed in Figure 3.5, the Na_2SO_4 electrolyte preserves a more ideal rectangular shape even at higher scan rates. This behavior suggests reduced polarization effects and more homogeneous ion adsorption across the electrode surface. The improved shape retention can be attributed to the stronger electrostatic interaction between divalent SO_4^{2-} ions and oxygen-containing functional groups present on the biochar surface, which stabilizes double-layer formation and promotes uniform charge distribution [8]. Additionally, sulfate ions tend to remain closer to the electrode interface due to stronger ion–surface interactions, reducing fluctuations in interfacial charge during rapid potential variation. In contrast, cyclic voltammograms obtained in $NaNO_3$ show slight distortion at higher scan rates, manifested as tilting and deviation from ideal rectangular geometry. As evidenced by the experimental curves in Figure 3.5, this distortion becomes more pronounced as scan rate increases, indicating growing kinetic limitations under fast polarization conditions. According to electrochemical theory, increasing scan rate reduces the time available for electrolyte ions to diffuse into smaller micropores, leading to partial utilization of the internal surface area [22]. Since NO_3^- ions are more mobile and weaker hydrated compared to SO_4^{2-}, they respond rapidly to potential changes, but also exhibit stronger sensitivity to diffusion gradients when polarization becomes fast.

The increase in current magnitude with scan rate observed for both electrolytes further confirms capacitive behavior. In ideal EDLC systems, current scales approximately linearly with scan rate because charge storage occurs through rapid ion rearrangement at the interface rather than slow diffusion-controlled reactions [4]. The proportional

current response seen in Figure 3.5 therefore indicates efficient double-layer formation and fast interfacial kinetics within the investigated potential window.

Overall, the cyclic voltammetry results demonstrate that both electrolytes enable predominantly EDLC-type charge storage, while electrolyte-dependent ion transport and interfacial interactions govern deviations from ideal behavior. The experimental observations presented in Figure 3.5 therefore confirm that electrolyte chemistry directly influences polarization behavior, rate capability, and accessibility of the porous biochar electrode surface.

3.7 Scan-Rate Dependence and Ion Transport

The dependence of specific capacitance on scan rate is illustrated in Figure 3.6, providing insight into the ion transport kinetics governing charge storage within walnut-shell-derived biochar electrodes.

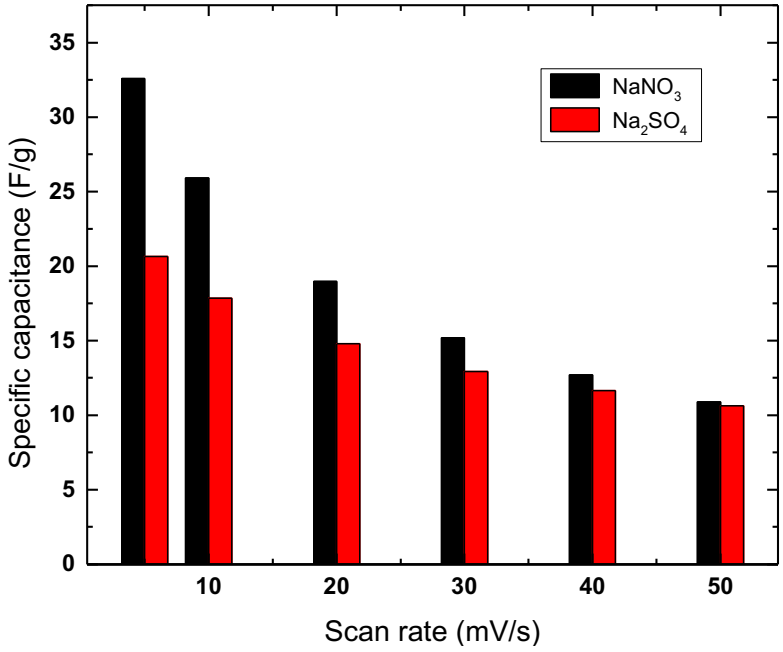


Figure 3.6: Specific capacitance variation as a function of scan rate for Na_2SO_4 and $NaNO_3$ electrolytes.

As shown in Figure 3.6, the specific capacitance decreases progressively with increasing scan rate for both electrolytes. This behavior is widely observed in porous carbon supercapacitors and is attributed to diffusion limitations that restrict ion accessibility to internal pore structures at high polarization rates [4], [6]. Similar scan-rate-dependent capacitance decay has been experimentally reported for biomass-derived carbon electrodes operating in aqueous electrolytes, where reduced ion diffusion time limits utilization of microporous surface area [23]. At low scan rates, the potential sweep occurs slowly, allowing sufficient time for solvated electrolyte ions to diffuse deeply into the hierarchical pore network. Under these conditions, both mesopores and micropores actively participate in charge storage, enabling nearly complete formation of the electrical double layer across the available surface area. Consequently, higher capacitance values are obtained, consistent with observations reported for porous biochar electrodes in sodium-based aqueous electrolytes [5]. As the scan rate increases, the characteristic diffusion time becomes shorter than the ion

transport time required to access narrow micropores. Charge storage therefore becomes increasingly confined to outer surfaces and larger pores, resulting in reduced effective capacitance. This transition from diffusion-controlled to surface-controlled charging has been experimentally demonstrated by Brousse et al. and further confirmed in porous carbon systems studied by Liu et al [4], [22].

Differences between Na_2SO_4 and $NaNO_3$ electrolytes observed in Figure 3.6 can be interpreted considering electrolyte-dependent ion transport properties. Electrolyte characteristics influence capacitance retention through ion hydration, mobility, and electrode–electrolyte interactions, as discussed by Pal et al [8]. Nitrate ions, characterized by lower charge density, respond more rapidly under slow polarization conditions, enabling higher capacitance at low scan rates. Conversely, sulfate ions exhibit stronger hydration and larger effective solvated size, which increases diffusion resistance within confined pores and enhances rate limitations at elevated scan rates.

The experimental trends obtained in this study therefore confirm that ion diffusion within the porous biochar framework governs scan-rate performance. The gradual reduction of capacitance with increasing scan rate reflects the intrinsic balance between ion transport kinetics and accessible surface area, supporting an electric double-layer dominated charge-storage mechanism consistent with previously reported aqueous carbon supercapacitor systems [6].

3.8 Kinetic Analysis Using the Power-Law Relationship

The electrochemical kinetics of walnut-shell-derived biochar electrodes were further analyzed using the power-law relationship:

$$i = av^b \quad (1)$$

where i represents the measured current, v is the scan rate, and a and b are adjustable parameters related to the charge-storage mechanism. This approach is widely used to distinguish between diffusion-controlled and surface-controlled electrochemical processes in supercapacitor electrodes [7].

The logarithmic form of the equation,

$$\log(i) = \log(a) + b\log(v) \quad (2)$$

allows determination of the kinetic parameter b from the slope of the linear log(i)–log(v) relationship. The corresponding plots obtained from the experimental data are presented in Figure 3.7.

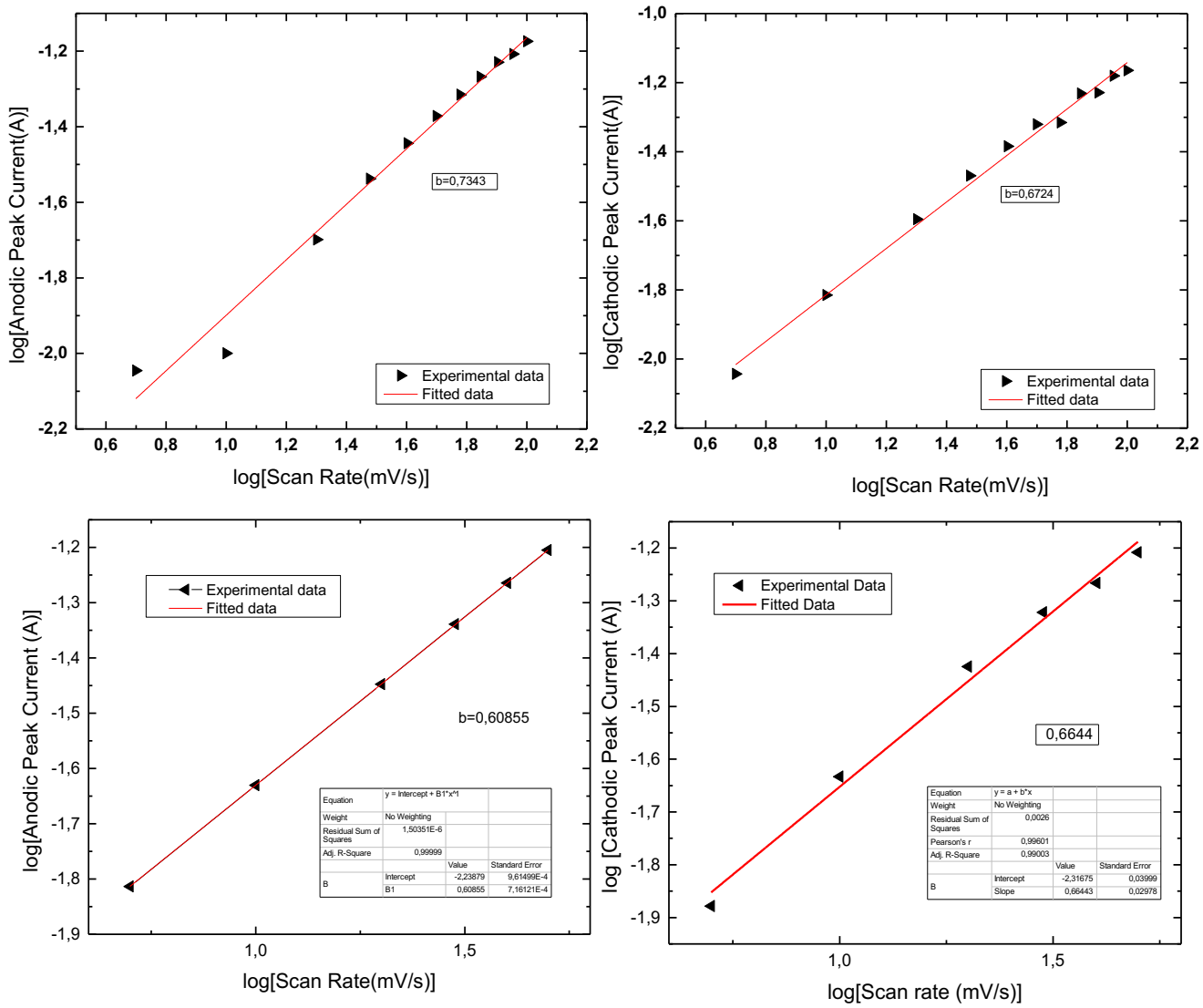


Figure 3.7: Log(i)–log(v) plots used for kinetic analysis ($i = av^b$). The upper graphs correspond to Na_2SO_4, while the lower graphs correspond to $NaNO_3$ electrolyte measurements.

As shown in Figure 3.7, the obtained relationships exhibit good linearity over the investigated scan-rate range, confirming that the electrochemical response follows power-law behavior typical of capacitive materials. The calculated *b*-values range between 0.6 and 0.73, indicating mixed-controlled kinetics involving both diffusion-controlled ion transport and surface-controlled capacitive processes. In electrochemical systems, a *b*-value close to 1 corresponds to ideal capacitive behavior dominated by surface-controlled charge storage, where current responds instantaneously to potential scan variation. Conversely, a value near 0.5 indicates diffusion-limited behavior governed by semi-infinite ion diffusion, typical of battery-type processes [7], [24]. The intermediate values obtained in this work therefore suggest that charge storage occurs primarily through electric double-layer formation with a measurable contribution from diffusion processes within the porous carbon structure.

The mixed kinetic behavior observed here is consistent with the hierarchical porosity of biomass-derived biochar electrodes [6]. During potential scan variation, ions initially accumulate rapidly at easily accessible external surfaces, producing a capacitive

response. Simultaneously, slower ion diffusion into micropores contributes additional charge storage, introducing diffusion-controlled characteristics into the overall current response [6].

A comparison between electrolytes reveals slightly higher slope values for Na_2SO_4, particularly during oxidation processes. This observation suggests improved accessibility or stabilization of electrochemically active sites under sulfate-based electrolyte conditions. Stronger electrostatic interactions between divalent SO_4^{2-} ions and oxygen-containing functional groups on the biochar surface may promote more uniform interfacial charge distribution, enhancing surface-controlled contributions to the current response [8]. In contrast, nitrate ions, although more mobile in bulk solution, exhibit greater sensitivity to diffusion gradients within confined pores during rapid polarization. This results in slightly lower *b*-values, reflecting a larger diffusion contribution to the overall kinetic response. Similar electrolyte-dependent variations in power-law kinetics have been reported for porous carbon electrodes in aqueous electrolytes, where ion hydration and transport properties modulate the balance between capacitive and diffusion-controlled processes [7].

Overall, the power-law analysis confirms that charge storage in walnut-shell-derived biochar electrodes is governed by a hybrid mechanism combining rapid surface-controlled adsorption with diffusion-assisted ion transport within the porous network. The experimentally determined *b*-values therefore provide quantitative evidence supporting the electric double-layer dominated behavior inferred from both cyclic voltammetry and galvanostatic charge–discharge analyses.

3.9 Diffusion- and Surface-Controlled Contributions

To further clarify the charge-storage mechanism of the biochar electrodes, the current response obtained from cyclic voltammetry was analyzed as a function of scan rate. This approach allows evaluation of the relative contributions of surface-controlled capacitive processes and diffusion-limited ion transport within the porous electrode structure.

According to Dunn's theory, current at a fixed potential related to the surface capacitive and diffusion-controlled process can be represented by the following equations [25], [26]:

$$i(V) = k_1 v + k_2 v^{1/2} \quad (3)$$

where $i(V)$ is the measured current at a specific potential, v is the scan rate, $k_1 v$ represents the surface-controlled capacitive current associated with rapid charge accumulation at the electrode surface, and $k_2 v^{1/2}$ corresponds to diffusion-controlled processes related to ion transport within the porous structure of the electrode .

To determine these contributions, the equation was rearranged into the linear form:

$$\frac{i(V)}{v^{1/2}} = k_1 v^{1/2} + k_2 \quad (4)$$

For each electrolyte, the current values extracted from the cyclic voltammetry curves at different scan rates were analyzed using this expression. Linear fitting of the experimental data allowed determination of the constants k_1 and k_2. These coefficients were then used to calculate the relative contributions of surface-controlled ($k_1 v$) and diffusion-controlled ($k_2 v^{1/2}$) currents at each scan rate. The resulting distributions are presented in Figure 3.8.

As shown in Figure 3.8a, the Na_2SO_4 electrolyte exhibits a progressively increasing diffusion-controlled contribution with increasing scan rate, indicating that charge storage becomes partially limited by ion transport within the porous biochar structure. This behavior is consistent with diffusion-regulated electrochemical processes typically observed in microporous carbon electrodes, where ion accessibility can be restricted by pore confinement and solvation effects [7].

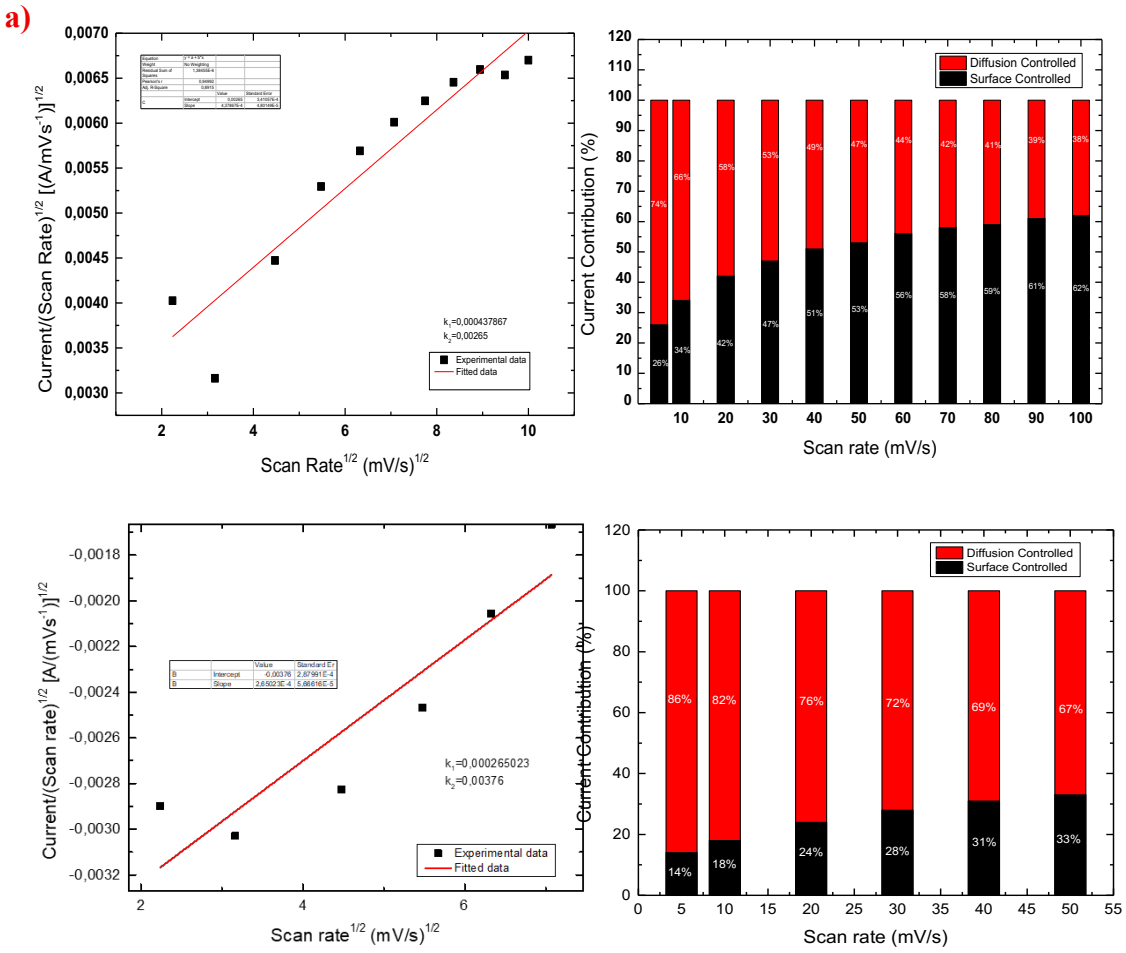


Figure 3.8: Quantitative separation of diffusion-controlled and surface-controlled current contributions derived from cyclic voltammetry analysis for **a)** Na_2SO_4 and **b)** $NaNO_3$ electrolytes.

In contrast, as shown in Figure 3.8b, the $NaNO_3$ electrolyte demonstrates a stronger surface-controlled contribution over the examined scan-rate range, suggesting that

charge storage occurs predominantly through rapid ion adsorption at readily accessible surface sites. Such behavior is often associated with electrolytes containing relatively mobile monovalent ions, which facilitate rapid formation of the electrical double layer at the electrode–electrolyte interface [4], [8].

The difference between the two electrolytes can therefore be interpreted as a consequence of ion charge density and hydration structure. Sulfate ions (SO_4^{2-}), being divalent and strongly hydrated, experience slower diffusion and stronger electrostatic interactions in confined pores, leading to increased diffusion limitations during rapid polarization. Conversely, nitrate ions (NO_3^-) exhibit weaker hydration shells and lower effective transport resistance, allowing faster establishment of interfacial charge storage. This interpretation agrees with electrolyte transport models demonstrating that ion solvation and confinement effects critically govern capacitive kinetics in porous carbons.

Overall, these findings demonstrate that electrolyte selection influences not only the magnitude of capacitance but also the charge-storage pathway and spatial distribution of stored charge within the electrode structure. The Na_2SO_4 system favors diffusion-assisted charge storage within the pore network, whereas $NaNO_3$ promotes rapid surface-controlled processes, highlighting the fundamental role of electrolyte chemistry in determining electrochemical kinetics.

3.10 EDLC and Pseudocapacitive Contributions

3.10.1 Separation of Charge-Storage Components

The charge-storage mechanism of the walnut-shell-derived biochar electrodes was further analyzed by estimating the relative contributions of electric double-layer capacitance (EDLC) and pseudocapacitive processes using the Trasatti method derived from cyclic voltammetry measurements.

According to this approach, the total capacitance of porous electrodes can be separated into surface-controlled and diffusion-related components by analyzing the scan-rate dependence of capacitance. The method is based on the following relationships [25], [27]:

$$\frac{1}{C} = \frac{1}{C_T} + kv^{1/2} \quad (5)$$

$$C = C_o + kv^{-1/2} \quad (6)$$

where C is the capacitance obtained from cyclic voltammetry measurements, $v$is the scan rate, $k$is a constant, C_T represents the total capacitance, and $C_o$corresponds to the electric double-layer capacitance.

To determine these parameters, the capacitance values obtained from cyclic voltammetry at different scan rates were plotted as 1/C versus $v^{1/2}$and C versus $v^{-1/2}$. Linear fitting of these plots allows the estimation of the total capacitance and the electric double-layer capacitance from the intercepts of the corresponding linear relationships. The difference between these values provides an estimate of the pseudocapacitive contribution. The resulting fitting plots for the investigated electrolytes are presented in Figure 3.9.

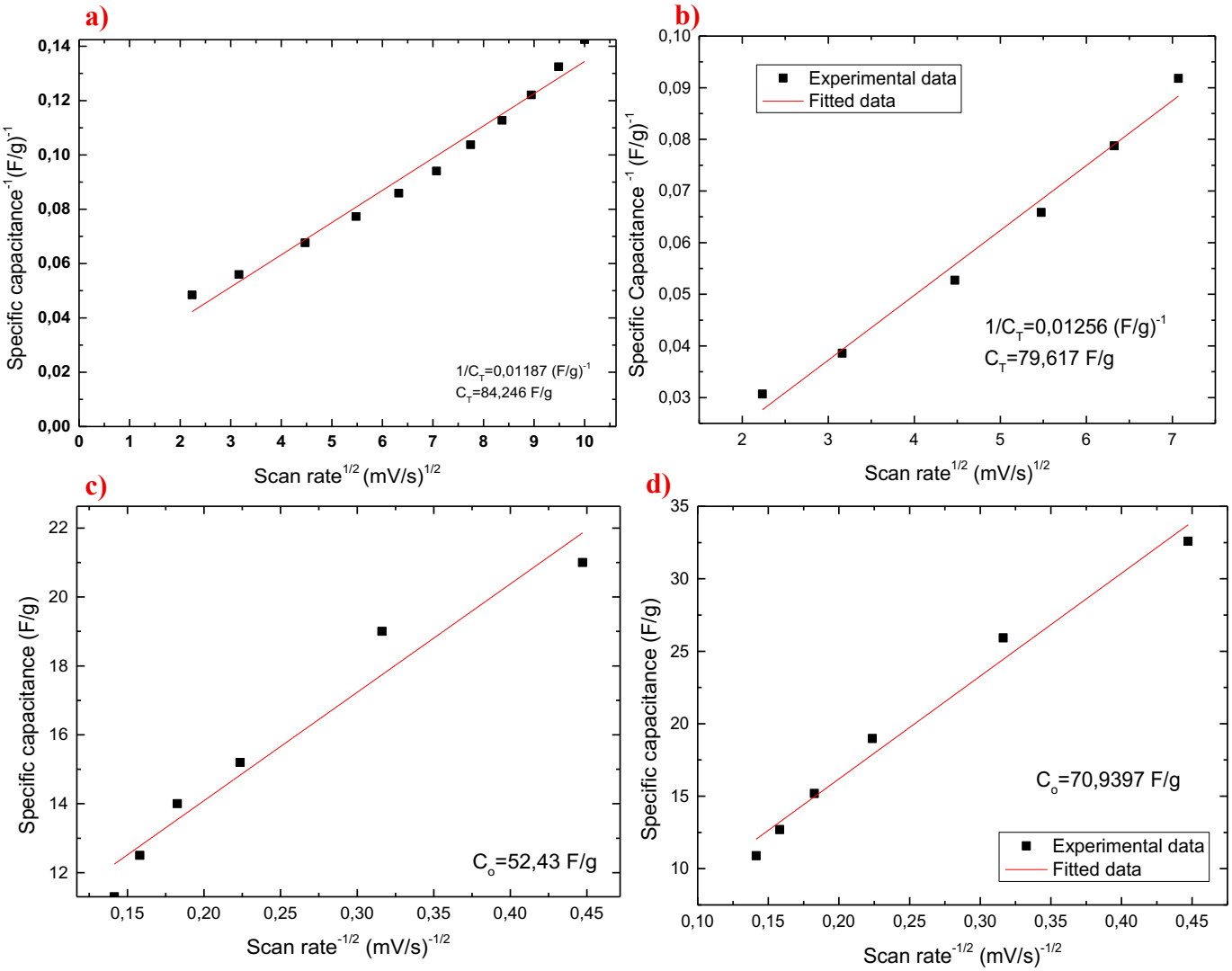


Figure 3.9 Determination of capacitance components from scan-rate analysis: **(a), (c)** Na_2SO_4 electrolyte and **(b), (d)** $NaNO_3$ electrolyte. Upper panels show linear fitting used for total capacitance extraction, while lower panels illustrate separation of EDLC and pseudocapacitive contributions.

As shown in Figures 3.9a and 3.9c, the electrodes operating in Na_2SO_4 electrolyte exhibit a total capacitance of approximately 84.25 F g^{-1}, consisting of 52.43 F g^{-1} electric double-layer capacitance and 31.82 F g^{-1} pseudocapacitive contribution. In contrast, the $NaNO_3$ electrolyte (Figures 3.9b and 3.9d) yields a slightly lower total capacitance (79.62 F g^{-1}), which is largely dominated by EDLC behavior (70.94 F g^{-1}) with a comparatively small pseudocapacitive contribution (8.68 F g^{-1}).

Electric double-layer capacitance originates from the electrostatic adsorption of ions at the electrode–electrolyte interface, forming a charge separation layer without faradaic reactions. In contrast, pseudocapacitance arises from fast reversible redox reactions or surface processes involving functional groups present on the carbon surface. The total capacitance can therefore be expressed as [25], [27]:

$$C_T = C_{EDLC} + C_P \quad (7)$$

Overall, these results indicate that electrolyte composition significantly influences the dominant charge-storage mechanism in the biochar electrodes. While the Na_2SO_4 electrolyte promotes a larger pseudocapacitive contribution, the $NaNO_3$ system favors charge storage primarily through electric double-layer formation.

3.10.2 Comparative Analysis of Electrolyte Influence

A direct comparison of the relative capacitance contributions was obtained using the capacitance components calculated from the equation (7) described in the previous section. Based on these values, the percentage participation of EDLC and pseudocapacitance was determined and is summarized in Figure 3.10, where the relative contributions of the two charge-storage mechanisms are illustrated for both electrolytes.

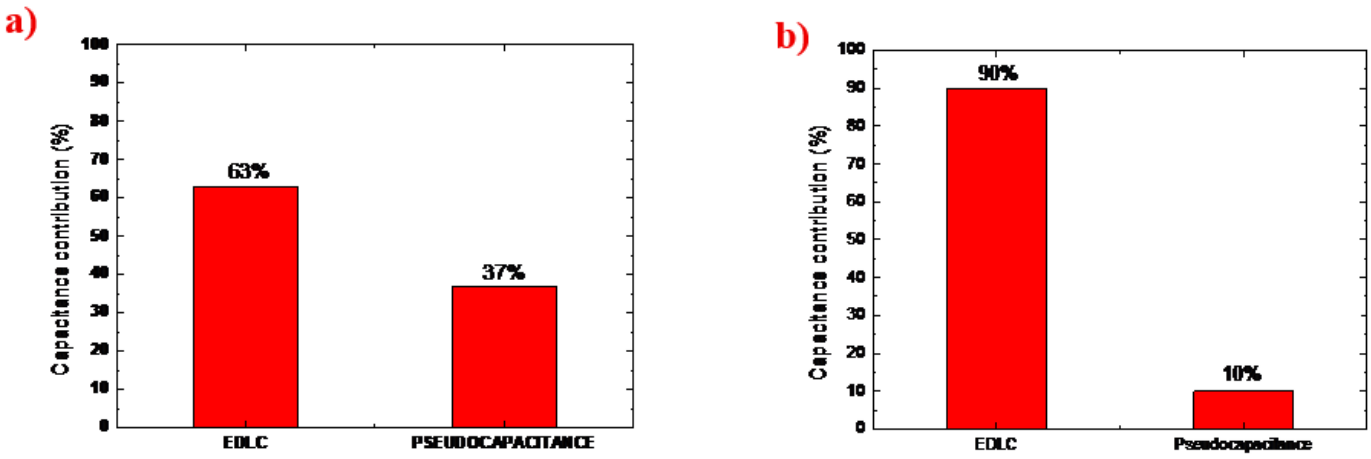


Figure 3.10 Relative contributions of electric double-layer capacitance and pseudocapacitance for walnut biochar electrodes: **(a)** Na_2SO_4 electrolyte and **(b)** $NaNO_3$ electrolyte.

The Na_2SO_4 system displays a balanced hybrid behavior, with approximately 63% EDLC and 37% pseudocapacitive contribution. This indicates that, beyond purely electrostatic charge accumulation, additional fast surface reactions significantly participate in energy storage. Conversely, the $NaNO_3$ electrolyte exhibits predominantly double-layer behavior, with nearly 90% of the stored charge originating from electrostatic adsorption processes.

The observed differences originate from fundamental electrolyte properties. Sulfate ions (SO_4^{2-}) possess higher charge density and stronger electrostatic interaction with oxygen-

containing functional groups naturally present on biomass-derived carbons. Such interactions may promote reversible surface redox processes and enhance pseudocapacitance, as reported for functionalized carbon electrodes [7], [24]. In contrast, nitrate ions (NO_3^-) are monovalent and chemically less interactive, favoring non-faradaic double-layer formation.

3.11 Discussion about Electrolyte-Dependent Charge Storage Mechanisms: Influence of Ion Chemistry, Conductivity, and pH

The electrochemical behavior of walnut-shell-derived biochar electrodes demonstrates a pronounced dependence on electrolyte chemistry, indicating that charge storage in aqueous carbon systems is governed by the coupled interaction between ion transport properties, electrolyte physicochemical characteristics, and electrode–electrolyte interfacial processes. The experimental observations presented throughout this chapter reveal that electrolyte selection controls not only the magnitude of capacitance but also the charge-storage mechanism operating within the porous electrode structure.

Higher specific capacitance values and longer discharge durations were consistently obtained in $NaNO_3$ electrolyte, indicating efficient ion transport and rapid establishment of the electrical double layer across a large fraction of the accessible surface area. The quasi-rectangular cyclic voltammograms and symmetric charge–discharge profiles further confirm that charge storage in this electrolyte is predominantly governed by EDLC. This behavior originates from the physicochemical characteristics of nitrate ions. As monovalent species with relatively low charge density, NO_3^- ions exhibit weaker ion–ion association and reduced hydration constraints compared with divalent sulfate ions. Consequently, ionic mobility in solution is enhanced, facilitating rapid migration toward the electrode surface and efficient penetration into microporous regions. Similar electrolyte-controlled transport effects have been widely reported for aqueous carbon-based supercapacitors, where ion mobility and hydration determine accessible surface utilization and rate capability [4], [8].

In contrast, Na_2SO_4 electrolyte produced slightly lower capacitance values, but exhibited significant pseudocapacitive participation, with approximately 37% of the total capacitance originating from surface-controlled processes. This hybrid behavior indicates stronger ion–surface interactions compared with the nitrate system. Sulfate ions (SO_4^{2-}), being divalent, possess higher charge density and stronger solvation shells. Although this reduces diffusion rates within narrow micropores, it increases electrostatic interaction strength at the electrode interface. As a result, ions remain longer near oxygen-containing functional groups naturally present on biomass-derived carbon surfaces, promoting reversible surface redox-like processes and enhancing pseudocapacitive contributions. Such electrolyte-induced modulation of storage mechanisms has been reported for functionalized carbon electrodes where ion valence governs the balance between electrostatic adsorption and surface faradaic processes [24].

Beyond ion valence and hydration effects, the electrochemical response observed in this study is strongly influenced by electrolyte conductivity. Ionic conductivity

determines the rate of charge transport within the electrolyte and directly affects internal resistance and electrode polarization. The relatively higher conductivity of $NaNO_3$ among neutral aqueous electrolytes facilitates rapid ion migration and minimizes ohmic losses, enabling efficient double-layer formation and improved rate performance. Increased electrolyte conductivity has been consistently correlated with enhanced capacitive behavior in porous carbon electrodes due to reduced polarization and faster charge propagation [6]. Although Na_2SO_4 exhibits comparable bulk conductivity, stronger ion–ion interactions and larger hydration structures increase the effective transport resistance under confinement. Consequently, ion diffusion becomes partially rate-limited within the porous network, promoting longer ion residence times near the electrode surface and enhancing pseudocapacitive contributions, as confirmed by the capacitance separation analysis.

The pH of the electrolyte constitutes an additional governing parameter influencing interfacial electrochemical behavior. Both Na_2SO_4 and $NaNO_3$ operate within near-neutral conditions (pH ≈ 7–8), providing chemically stable environments that preserve surface functional groups and suppress parasitic reactions. Under these conditions, charge storage occurs predominantly through reversible ion adsorption and surface-confined processes. Slightly higher pH values measured for $NaNO_3$ promote partial deprotonation of oxygen-containing functional groups, increasing surface charge density and facilitating electrostatic ion adsorption, thereby reinforcing EDLC-dominated behavior. In contrast, strongly alkaline electrolytes such as NaOH (pH ≈ 14) promote water decomposition and gas evolution at relatively low overpotentials, leading to polarization effects and unstable electrochemical performance, as experimentally observed. High hydroxide concentration can also modify surface charge distribution through specific adsorption, disrupting reversible charge-storage processes [22]. Similarly, despite adequate conductivity, NaCl electrolyte exhibited poor compatibility due to chloride-induced corrosion phenomena affecting metallic components, demonstrating that electrolyte suitability depends on the combined influence of conductivity, pH, and chemical reactivity rather than conductivity alone.

The scan-rate dependence and kinetic analyses further support this mechanistic framework. Increasing diffusion-controlled contributions observed for Na_2SO_4 indicate progressive ion penetration into the porous network, whereas $NaNO_3$ exhibits increasingly surface-dominated behavior at higher rates. These results demonstrate that electrolyte chemistry determines how charge is spatially distributed within the electrode:

- $NaNO_3$ promotes rapid ion transport and extensive surface utilization, resulting in EDLC-dominated storage.
- Na_2SO_4 enhances interfacial interactions, producing hybrid EDLC/pseudocapacitive behavior.

Overall, the electrochemical performance of walnut-derived biochar electrodes emerges from the dynamic coupling between pore architecture, surface chemistry, electrolyte conductivity, and solution pH. The results demonstrate that electrolyte engineering represents a critical strategy for tuning charge-storage mechanisms in sustainable

aqueous energy-storage systems, providing a coherent mechanistic framework linking electrolyte physicochemical properties with electrochemical response.

3.12 References

[1] H. H. U. R. Winston Revie, Corrosion and Corrosion Control: An Introduction to Corrosion Science and Engineering, 2008.

[2] H. S. A. e. al., «Influence of Chloride Ions on Electrochemical Corrosion Behavior of Dual-Phase Steel over Conventional Rebar in Pore Solution,» *Applied Sciences,* 2020.

[3] H. P. e. al., «A review of passivity breakdown on metal surfaces: influence of chloride- and sulfide-ion concentrations, temperature, and pH,» *ResearchGate,* 2021.

[4] L. L. Z. e. al., «Carbon-based materials as supercapacitor electrodes,» *Chemical Society Reviews,* 2009.

[5] E. F. e. al., «Carbon materials for the electrochemical storage of energy in capacitors,» *ScienceDirect, vol*. 39, issue 6, pp. 937-950, 2001.

[6] P. S. &. Y. Gogotsi, «Materials for electrochemical capacitors,» *Nature Materials,* pp. 845–854, 2008.

[7] B. D. e. al., «Electrical Energy Storage for the Grid: A Battery of Choices,» *Science, vol*. 334, issue 6058, pp. 928-935, 2011.

[8] B. P. e. al., «Electrolyte selection for supercapacitive devices: a critical review,» *Royal Society of Chemistry,* pp. 3807-3835, 2019.

[9] D. L. S. J. F. M. Lu Guan, «Structural Regulation and Performance Enhancement of Carbon-Based Supercapacitors: Insights into Electrode Material Engineering,» *Materials, vol*. 18, 2025.

[10] Z. M. S. A. Q. A. Zhazira Supiyeva, «A unique choline nitrate-based organo-aqueous electrolyte enables carbon/carbon supercapacitor operation in a wide temperature window (−40°C to 60°C),» *frontiers in Chemistry,* 2024.

[11] Y. A. M. M. F. I. Tatsuya Iida, «Effect of surface property of activated carbon on adsorption of nitrate ion,» *PubMed,* 2013.

[12] K. F. e. al., «Effect of surfactants on capacitance properties of carbon electrodes,» *Electrochimica Acta, vol*. 60, 2012.

[13] C. P. Y. J. Lili Dong, «Corncob-Derived Activated Carbon as Electrode Material for High-Performance Supercapacitor,» *Materials,* 2024.

[14] K. Q. e. al., «Recent advances in utilization of biochar,» *Renewable and Sustainable Energy Reviews, vol*. 42, pp. 1055-1064, 2015.

[15] Z. Q. e. al., «Biochar-based carbons with hierarchical micro-meso-macro porosity for high rate and long cycle life supercapacitors,» *Journal of Power Sources,* 2018.

[16] T. F. D. K. C. Q. J. Long Ye, «Can Aqueous Na2SO4-Based Neutral Electrolyte Increase Energy Density of Monolithic Wood Biochar Electrode Supercapacitor?,» *Energies,* 2024.

[17] J. F. e. al., «Symmetric supercapacitors with cellulose-derived carbons and Na2SO4 electrolytes operating in a wide temperature range,» *Journal of Energy Storage,* 2022.

[18] S. A. e. al., «Walnut shell derived N, S co-doped activated carbon for solid-state symmetry supercapacitor device,» *Journal of Industrial and Engineering Chemistry, vol*. 129, pp. 309-320, 2024.

[19] M. R. P. e. al, «High-performance aqueous sodium-ion storage using bundled fiber-based electrodes,» *Journal of Materials Chemistry A, vol*. 18, 2025.

[20] P. L. &. V. B. T. P. Nghia Trong Nguyen, «Biomass-derived activated carbon electrode coupled with a redox additive electrolyte for electrical double-layer capacitors,» *Journal of Nanoparticle Research, vol*. 22, 2020.

[21] J. A. e. al, «Activated Biocarbon from Paper Mill Sludge as Electrode Material for Supercapacitors: Comparative Performance Evaluation in Two Aqueous Electrolytes,» *ACS Omega, vol*. 8, 2023.

[22] T. B. e. al., «To Be or Not To Be Pseudocapacitive?,» *IOP Publishing and The Electrochemical Society,* 2015.

[23] D. L. e. al., «Porous carbons derived from waste printing paper for high rate performance supercapacitors in alkaline, acidic and neutral electrolytes,» *Royal Society of Chemistry,* pp. 3974-3981, 2018.

[24] V. A. e. al., «High-rate electrochemical energy storage through Li+ intercalation pseudocapacitance,» *Nature Materials,* 2013.

[25] M. K. e. al., «A rational preparation strategy of phase tuned MoO3 nanostructures for high-performance all-solid asymmetric supercapacitor,» *Journal of Energy Chemistry, vol*. 87, pp. 192-206, 2023.

[26] M. K. S. S. S. S. S. J. Biswarup Gourd, «Fabrication of multiwalled carbon nanotube decorated two dimensional CuO nanosheets with high charge storage capacity and excellent cyclic stability for supercapacitor applications,» *Diamond and Related Materials, vol*. 159, 2025.

[27] A. V. S. S. &. B. P. Jayant Yadav, «Role of oxidation states of iron on the super-capacitive behaviour of iron oxide films,» *Applied Physics A, vol*. 128, 2022.

[28] A. A.-M. e. al, «Coffee-derived activated carbon from second biowaste for supercapacitor applications,» *Waste Management, vol*. 120, pp. 280-289, 2021.

Chapter 4. Two-Electrode System Cell: Electrochemical Analysis

The electrochemical performance of walnut-shell-derived biochar electrodes was evaluated using a symmetric two-electrode configuration to assess the practical behavior of the assembled device. In contrast to the three-electrode analysis presented in Chapter 3, this configuration reflects the total cell response, including internal resistance and electrolyte transport effects.

4.1 Galvanostatic Charge–Discharge Performance in the Two-Electrode Configuration

Galvanostatic charge–discharge measurements were conducted within a voltage window of 0–1 V at specific currents between 0.1 and 0.5 A g^{-1} using Na_2SO_4 and $NaNO_3$ aqueous electrolytes.

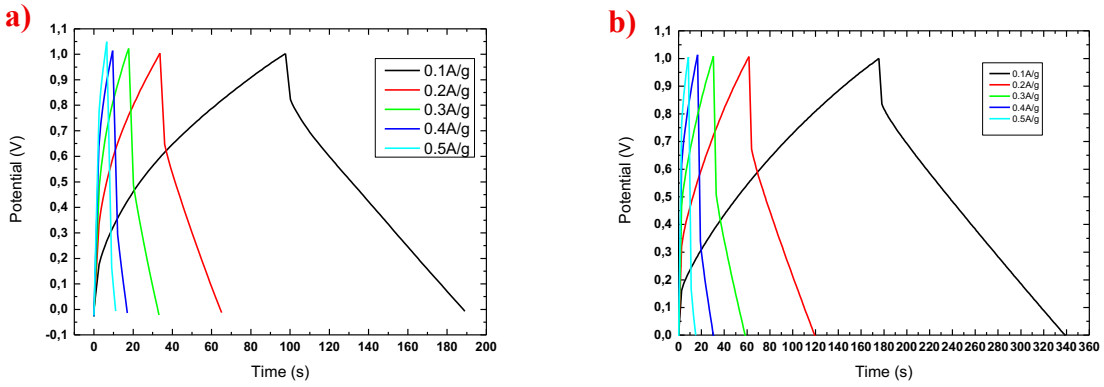


Figure 4.1: Galvanostatic charge–discharge curves of symmetric walnut biochar cells measured at different specific currents in **(a)** Na_2SO_4 and **(b)** $NaNO_3$ electrolytes. Προσοχή στη γραμματοσειρά

As shown in Figure 4.1, both systems display nearly linear voltage–time profiles characteristic of capacitive behavior. $NaNO_3$ exhibits longer discharge times, reaching approximately 340 s at 0.1 A g^{-1}, indicating higher cell capacitance at low specific current. In contrast, Na_2SO_4 presents more symmetric charge–discharge curves, suggesting lower polarization and improved reversibility. At higher specific currents, increased distortion is observed for $NaNO_3$, indicating stronger polarization effects under fast charging conditions.

4.2 Specific Cell Capacitance Comparison in the Two-Electrode System

The variation of specific cell capacitance with specific current for the symmetric two-electrode configuration is presented in Figure 4.2.

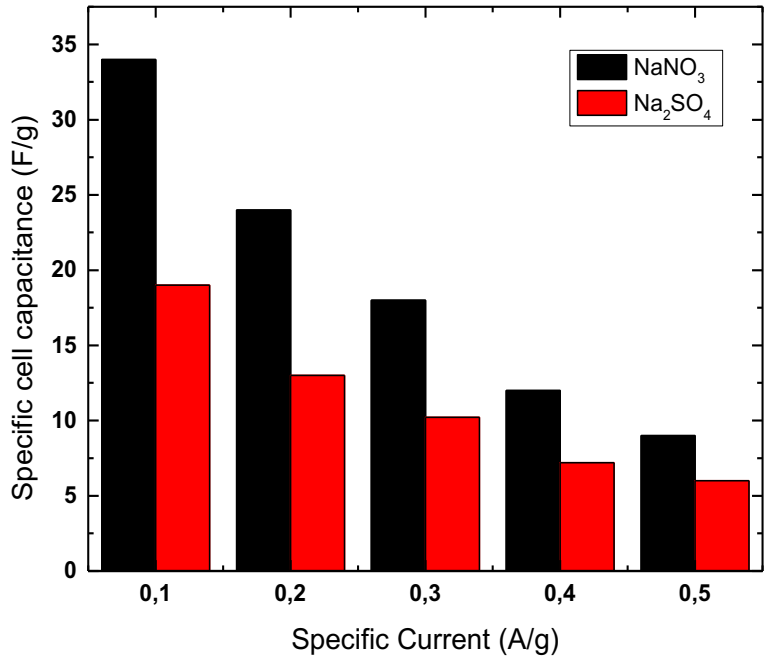


Figure 4.2: Specific cell capacitance as a function of specific currentfor symmetric walnut biochar cells operating in Na_2SO_4 and $NaNO_3$ electrolytes.

As shown in Figure 4.2, both electrolyte systems exhibit a progressive decrease in specific capacitance with increasing specific current, which is typical for porous carbon electrodes operating under galvanostatic conditions, where ion transport limitations become increasingly significant at higher charge–discharge rates. Experimentally, the capacitance of the Na_2SO_4 system decreases from 19 to 6 F g^{-1} as the specific current increases from 0.1 to 0.5 A g^{-1}, while the $NaNO_3$ electrolyte shows higher overall values, decreasing from 34 to 9 F g^{-1} over the same range.

The higher capacitance observed for $NaNO_3$ at low specific current indicates more efficient ion accessibility and rapid establishment of charge storage within the electrode structure under slow operating conditions. Nevertheless, Na_2SO_4 demonstrates a smaller relative loss of capacitance as specific current increases, suggesting improved rate stability and more uniform utilization of the electrochemically active material when faster charge propagation is required. This behavior highlights the different operational responses of the two electrolytes in a practical device configuration, where electrolyte properties influence the balance between achievable energy storage and performance retention at elevated current loads.

4.3 Comparative Cyclic Voltammetry Analysis

Cyclic voltammetry measurements were conducted to further evaluate reversibility and capacitive behavior of the assembled devices.

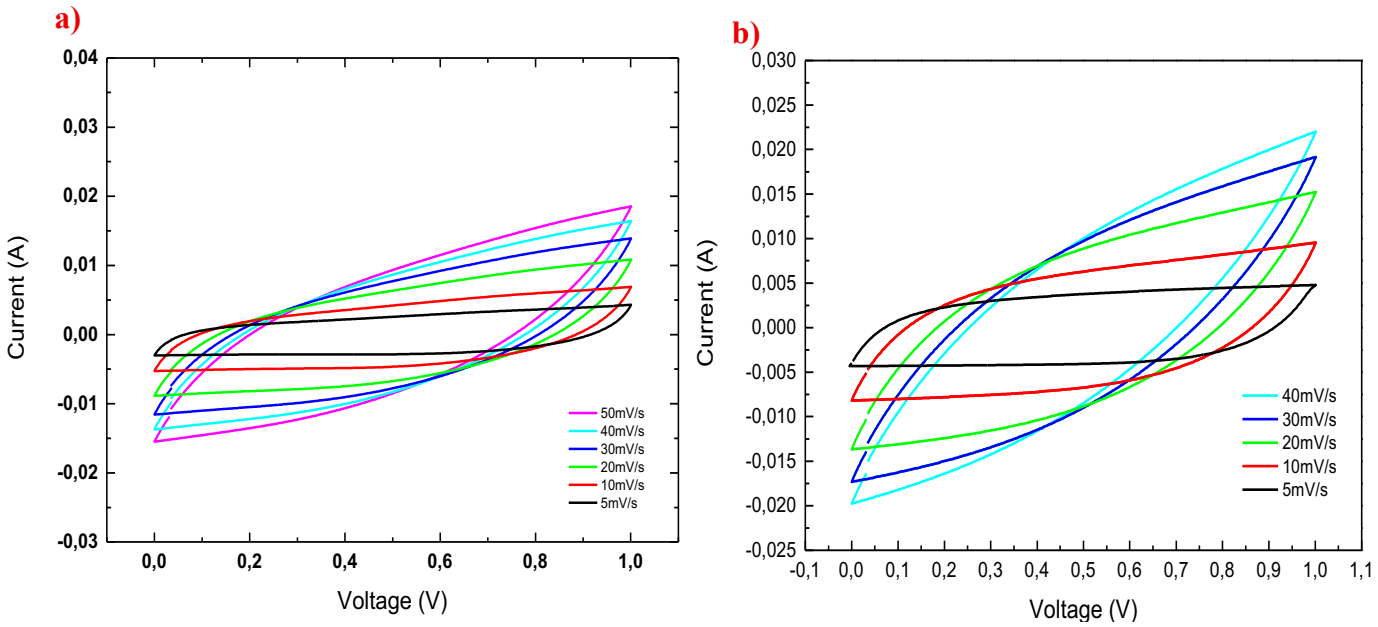


Figure 4.3: Cyclic voltammograms of symmetric walnut biochar cells recorded at different scan rates in **(a)** Na_2SO_4 and **(b)** $NaNO_3$ electrolytes.

Both systems display characteristic capacitive behavior; however, notable differences emerge as the scan rate increases. As shown in Figure 4.3, the Na_2SO_4 electrolyte maintains more rectangular and symmetric CV profiles across all scan rates, indicating stable ion adsorption processes and reduced polarization effects within the investigated voltage window. In contrast, the $NaNO_3$ system exhibits higher current response at low scan rates but progressively distorted CV loops at higher scan rates, suggesting increased internal resistance and kinetic limitations under rapid potential variation.

The deviation from the ideal rectangular shape reflects incomplete ion diffusion and delayed charge propagation at elevated scan rates, consistent with the polarization behavior previously observed in the galvanostatic charge–discharge measurements.

4.4 Cycling Stability and Coulombic Efficiency Analysis

The long-term electrochemical stability of the symmetric walnut-biochar supercapacitor cells was evaluated through repeated charge–discharge cycling in order to assess device durability under realistic operating conditions. Stability measurements were performed for both Na_2SO_4 and $NaNO_3$ aqueous electrolytes using galvanostatic cycling and cyclic voltammetry analysis.

The evolution of electrochemical performance during prolonged cycling in Na_2SO_4 electrolyte is presented in Figure 4.4.

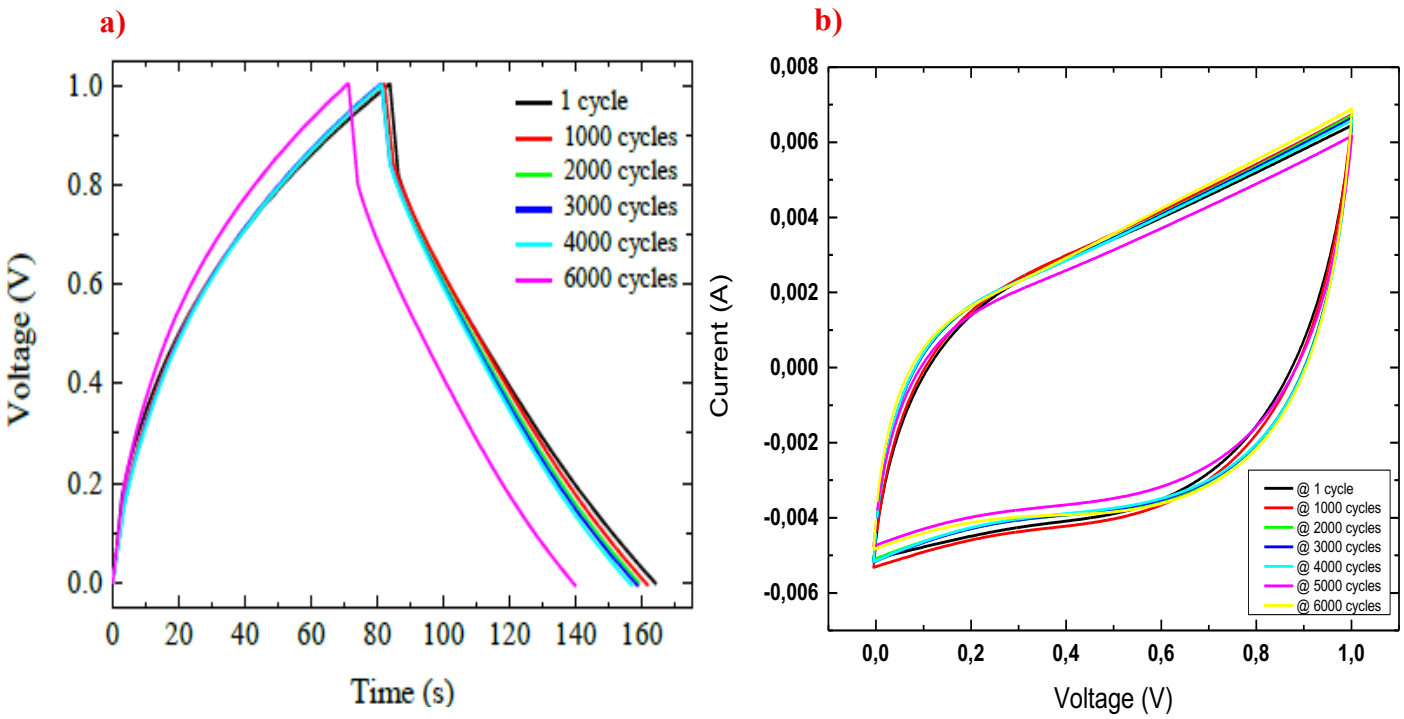


Figure 4.4: Cycling stability of symmetric walnut biochar cells in Na_2SO_4 electrolyte showing **(a)** galvanostatic charge–discharge curves and **(b)** cyclic voltammograms recorded at different cycle numbers.

As shown in Figure 4.4a, the galvanostatic charge–discharge profiles remain nearly unchanged throughout cycling, indicating highly reversible electrochemical behavior. The preservation of symmetric voltage–time characteristics demonstrates stable ion adsorption and limited increase in internal resistance. The cyclic voltammograms in Figure 4.4b further confirm stable capacitive response with minimal distortion after extended cycling.

The cycling stability was quantified using the capacitance retention, calculated according to:

$$\text{Capacitance Retention (\%)} = \frac{C_{\text{final}}}{C_{\text{initial}}} \times 100\%$$

where C_{initial} corresponds to the specific capacitance of the first cycle and C_{final} represents the capacitance after prolonged cycling.

Based on the experimental measurements, the capacitance decreases slightly from approximately 19 F g^{-1} in the first cycle to about 17 F g^{-1} after 6000 cycles, corresponding to a capacitance retention of approximately 90%, as is presented in Figure 4.5 demonstrating excellent electrochemical durability in the sulfate electrolyte.

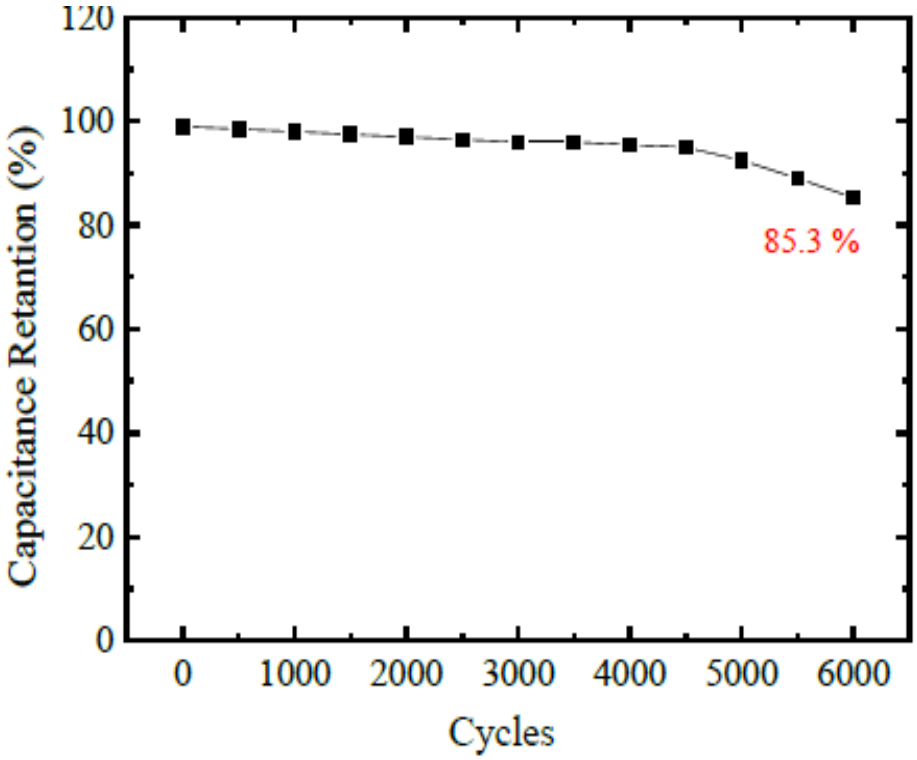


Figure 4.5: Capacitance retention (%) as a function of charge–discharge cycling number, demonstrating the cycling stability of the electrode material over 6000 cycles, with a final capacitance retention of approximately 85.3%, indicating good long-term electrochemical stability.

As illustrated in Figure 4.6a, progressive shortening of discharge time is observed during cycling, indicating capacitance fading for the measurements in $NaNO_3$ electrolyte. The CV profiles shown in Figure 4.6b display reduced current response compared to the first cycle, suggesting increasing polarization and loss of electrochemically accessible surface area. Using the same retention equation presented above, the specific capacitance decreases from approximately 34 F g^{-1} in the first cycle to nearly 16 F g^{-1} after 400 cycles, yielding a capacitance retention of approximately:

$$\frac{16}{34} \times 100 \approx 47\%$$

This substantial decrease indicates reduced long-term stability despite the initially higher capacitance delivered by the nitrate electrolyte.

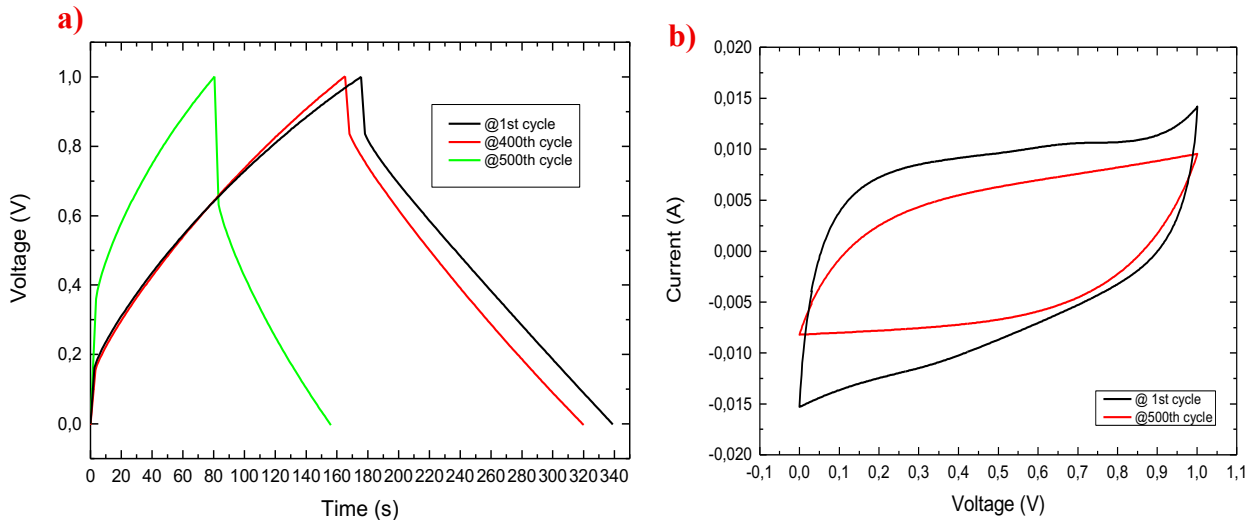


Figure 4.6: Cycling stability of symmetric walnut biochar cells in $NaNO_3$ electrolyte showing **(a)** evolution of galvanostatic charge–discharge curves and **(b)** cyclic voltammetry response during cycling.

Overall, the stability analysis reveals a clear electrolyte-dependent trade-off between initial capacitance and long-term durability. While $NaNO_3$ provides higher initial capacitance, Na_2SO_4 maintains superior cycling stability and structural integrity over extended operation. These results demonstrate that electrolyte selection critically governs practical device lifetime in symmetric aqueous supercapacitors.

4.5 Comparison with Literature and Performance Benchmarking

To evaluate the practical electrochemical performance of the walnut-shell-derived biochar supercapacitor developed in this work, a comparison with previously reported biomass-derived carbon electrodes tested in aqueous sodium-based electrolytes was conducted. Particular emphasis is placed on results obtained in symmetric two-electrode configurations, as these measurements represent the actual operating conditions of supercapacitor devices.

While many literature studies report electrochemical performance using three-electrode configurations for fundamental material characterization, the practical performance of supercapacitors is more accurately assessed using two-electrode systems. In a symmetric two-electrode configuration, both electrodes participate in charge storage and the measured capacitance reflects the performance of the full device rather than the intrinsic behavior of a single electrode.

In the present study, the walnut-shell-derived biochar electrodes were evaluated in a symmetric two-electrode supercapacitor configuration using neutral aqueous electrolytes. The device exhibited a specific capacitance of approximately 19 F g^{-1} in 1 M Na_2SO_4 electrolyte and 64.2 F g^{-1} in 1 M $NaNO_3$ electrolyte. The higher capacitance observed in the nitrate-based electrolyte is consistent with the improved ion transport and accessibility previously discussed, which enhance effective charge storage within the porous carbon structure.

When compared with biomass-derived carbon electrodes reported in the literature under similar aqueous conditions, the performance of the biochar-based device developed in this work falls within the expected range for symmetric aqueous supercapacitors. For

example, activated coffee-derived biochar electrodes have been reported to deliver capacitance values of approximately 89 F g^{-1} in Na_2SO_4 electrolytes [1], while activated wood-derived biochar electrodes typically exhibit capacitances around 46 F g^{-1} in similar symmetric device configurations [2] .Although these materials often achieve higher capacitance values, their performance is typically associated with chemical activation treatments that significantly increase surface area and pore development.

In contrast, the walnut-shell biochar electrodes investigated in this work were synthesized without chemical activation, resulting in a considerably simpler and more environmentally sustainable preparation process. Despite the absence of activation, the symmetric biochar-based device demonstrates competitive electrochemical behavior, particularly in $NaNO_3$ electrolyte, where the measured capacitance of 64.2 F g^{-1} approaches the performance of several activated biomass-derived carbons reported in the literature.

An important parameter for practical supercapacitor applications is long-term cycling stability. In the present work, the symmetric biochar-based device operating in Na_2SO_4 electrolyte maintained approximately 90% capacitance retention after 6000 charge–discharge cycles, indicating excellent electrochemical durability. Such cycling stability is comparable to, or even exceeds, that reported for several activated biomass-derived carbon electrodes under similar aqueous conditions. The high stability observed suggests that the structural integrity of the walnut-shell-derived biochar electrode remains largely preserved during repeated charge–discharge processes.

Overall, the comparison with literature demonstrates that the walnut-shell-derived biochar developed in this study exhibits reliable and competitive performance when evaluated under practical device conditions. Although chemically activated carbons frequently achieve higher capacitance values due to their highly developed porous structures, the results obtained in this work indicate that activation-free biomass-derived carbons can still provide effective energy-storage performance when combined with appropriate electrolyte selection and electrode fabrication strategies. In particular, the improved performance observed in $NaNO_3$ electrolyte highlights the important role of electrolyte chemistry in optimizing the operation of sustainable carbon-based supercapacitor devices.

These findings support the potential of walnut-shell-derived biochar as a low-cost, environmentally friendly electrode material for aqueous supercapacitors, offering a promising pathway toward sustainable and scalable energy-storage technologies.

4.6 References

[1] A. A.-M. e. al, «Coffee-derived activated carbon from second biowaste for supercapacitor applications,» *Waste Management, vol*. 120, pp. 280-289, 2021.

[2] Y. L. e. al., «Can Aqueous Na2SO4-Based Neutral Electrolyte Increase Energy Density of Monolithic Wood Biochar Electrode Supercapacitor?», *Energies,* 2024.

Chapter 5. Conclusions

This thesis investigated the electrochemical performance of walnut-shell-derived biochar electrodes as sustainable carbon materials for aqueous sodium-based energy storage systems. The study aimed to clarify how electrolyte chemistry influences charge-storage mechanisms, ion transport behavior, and practical device performance using both three-electrode and symmetric two-electrode configurations.

Walnut shells were successfully converted into carbon electrodes through a simple pyrolysis process at 800 °C without chemical or physical activation, demonstrating a low-cost and environmentally sustainable synthesis route. Despite the absence of activation, the produced biochar exhibited sufficient electrochemical activity and mechanical stability, confirming the feasibility of utilizing minimally processed biomass-derived carbons for energy-storage applications.

Electrochemical characterization in the three-electrode configuration revealed a dependence of electrode behavior on electrolyte ingredients. Among the investigated sodium-based electrolytes, NaCl and NaOH showed limited compatibility due to corrosion phenomena and polarization effects associated with alkaline environments. In contrast, neutral electrolytes enabled stable operation and allowed systematic investigation of charge-storage mechanisms. Comparative analysis demonstrated that $NaNO_3$ electrolyte promoted higher specific capacitance values due to enhanced ion mobility and efficient electric double-layer formation, whereas Na_2SO_4 induced hybrid charge-storage behavior involving both double-layer and surface-controlled contributions. These findings confirmed that electrolyte chemistry governs not only capacitance magnitude, but also interfacial electrochemical processes within porous biomass-derived carbons.

Evaluation in a symmetric two-electrode configuration provided insight into realistic device performance. Although the $NaNO_3$ electrolyte delivers higher initial capacitance values, its limited electrochemical stability leads to progressive capacitance fading during prolonged cycling. In contrast, the Na_2SO_4 electrolyte exhibits superior electrochemical robustness, enabling operation at higher specific currents while maintaining stable cycling performance. The symmetric cell retained approximately 90% of its initial capacitance after 6000 cycles, demonstrating excellent durability under repeated charge–discharge conditions. Electrochemical impedance analysis further confirmed favorable interfacial kinetics and a near-ideal capacitive response for the Na_2SO_4-based system, indicating reduced charge-transfer resistance and stable electrode–electrolyte interaction during long-term operation.

Overall, the results demonstrate that electrochemical performance arises from the coupled interaction between cell assembly and electrolyte physicochemical properties, including ion valence, hydration behavior, conductivity, and pH. The walnut-shell biochar electrodes exhibit tunable charge-storage mechanisms depending on electrolyte selection, highlighting electrolyte as a key parameter for optimizing aqueous sodium-based energy-storage systems.

This work demonstrates that activation-free biomass-derived carbons can achieve competitive electrochemical performance while preserving advantages of

sustainability, low cost, and scalability. The findings contribute to a deeper understanding of electrolyte–electrode interactions in aqueous supercapacitors and support the development of environmentally responsible carbon materials for next-generation energy storage technologies.

Chapter 6. Future Perspectives and Research Directions

Future research efforts will aim to further enhance the electrochemical performance of walnut-shell-derived biochar electrodes and reduce the performance gap relative to highly activated carbon materials. Potential strategies include tailoring the pore structure through controlled activation procedures to increase specific surface area and develop hierarchical porosity that facilitates improved ion transport. In addition, the incorporation of heteroatom dopants may promote additional pseudocapacitive contributions while improving surface wettability and electrode–electrolyte interaction.

Optimization of electrode architecture, particularly mass loading and electrode thickness, also represents an important pathway toward improving practical device-level capacitance. Moreover, investigation of alternative neutral sodium-based electrolytes or hybrid aqueous electrolyte systems could provide a more favorable balance between high initial capacitance and long-term cycling stability. These approaches are expected to enhance ion accessibility within the porous network, improve charge-storage efficiency, and strengthen rate capability.

Overall, such developments could bring walnut-shell-derived biochar electrodes closer to the performance levels typically achieved by highly activated carbons, while maintaining the sustainability, and scalability for environmentally responsible energy-storage applications.